Proceedings of International Conference
Applications of Structural Fire Engineering
Prague, 19-20 February 2009

Session 3

Material Modelling

MATERIAL PROPERTIES LOSS OF FIBRED-SCC DUE TO FIRE ACTION

Alonso, C. and Rodriguez, C.

Eduardo Torroja Institute of Construction Sciences (IETcc) – CSIC ,Madrid, Spain

INTRODUCTION

Traditionally concrete is identified as a material showing good resistance against fire, but it is also known that different changes take place in chemical composition, pore structure and water content when concrete is exposed to high temperatures, that together with thermal expansions finally produce losses in mechanical strength properties [1, 2]. Furthermore other type of damage exists that affects the integrity of the structure under fire, associated with a type of explosion. The risk of spalling of concrete at high temperature implies reduction of the effective section and concrete cover, and facilitates the exposure of new faces of concrete to the high temperatures developed during the fire [3].

High dense concretes, as high and ultra high strength concretes, are more prone to spalling when exposed to high temperatures than normal concretes, the reason is associated with the fineness of the pore structure that does not facilitate the water vapour easily to be evacuated, what induces increase of the vapour pressures inside the pores and then the risk of spalling [4]. In addition SCC is also considered to show less fire resistance [5-8], although no agreement between authors is found. A challenge appears trying to understand the mechanism of spalling to allow more efficient design of new concretes.

Experiences with high strength concrete reinforced with polypropylene fibers have showed that a certain favourable effect is noticed to reduce the spalling risk of the concrete cover, although some fails have indicated that the risk still remains and the reason is not yet well understood, it would depend on the dosage and type of fibers used [9-15].

Present work focuses on mechanical and microstructure properties evolution under fire of self compacting concrete (SCC) and the modification due to fibers addition, polypropylene and steel, used separately or mixed, in order to analysed the response at high temperatures and the influence of the type of fibre.

1 EXPERIMENTAL PROGRAM

1.1 Materials

Self-Compacting Concrete was manufactured with 426 kg/m^3 of Ordinary Portland Cement (OPC) (CEM I 52.5 R), 963 kg/m^3 of crushed limestone aggregates with a grading of 0-5 mm for the sand and 5/12 mm for the gravel, 647 kg/m^3 of limestone filler and 6.40 kg/m^3 of polycarboxylate-based superplasticizer, the water/cement ratio (w/c) was 0.45.

Additions of fibers were also used in several proportions: 1) 3 kg/m^3 of polypropylene (PPF) of 54 mm of length and 0.05 mm of diameter, 2) 40kg/m^3 of steel fiber (SF) with 30mm of length and 0.48mm of diameter, and 3) mix of PPF + SF, 1.5 kg/m^3 and 20kg/m^3 respectively.

Beams of 40x10x10cm were fabricated, but tests were carried out using cylindrical cores of 7.5x10 cm taken from the beams.

1.2 Test method

The SCC concrete cores were exposed to several temperatures in an electrical furnace and heated at a heating rate of 2ºC/min until the temperature selected and maintained for two hours. Then, the cooling of the samples was allowed inside the furnace, following a cooling rate <1ºC/min.

After cooling, in residual state, changes in microstructure and mechanical properties of the heated concrete samples were measured.

The temperatures considered were: 20ºC (as initial), 200, 300, 500, 700 and 1200 ºC: After heating, each specimen was introduced in a plastic bag and then in a box free of humidity and CO_2 to avoid any negligible effect due to contact with the atmosphere before testing. The characterisation tests were:

- *Residual mechanical properties*: Compressive strength and indirect tensile strength.
- *Pore structure:* Total porosity and pore size distribution using mercury porosimetry.
- *TG/DTA:* Transformations taking place in hydrated phases of cement paste and aggregates of SCC and in the PPF fiber.
- *Microscopy:* to determine the microstructure in pore density, microcracks and dehydrated phases distribution using back-scattered-SEM and stereoscopic microscopy.

2 RESULTS AD DISCUSSION

2.1 Chemical composition changes in SCC after exposure to high temperatures

The transformations occurring in chemical composition of hydrated phases in SCC at high temperatures have been identified using thermo-gravimetric tests (TG/DTA) in samples previously exposed to several temperatures (20, 105, 300, 500, 700 and 1200ºC) are included in *Fig.1-left* and in *Table 1*. The results follow similar performance than a conventional cement paste up to temperatures of 500ºC, as indicated in [2]. The main differences appear in temperatures > 600ºC, showing higher weight losses associated to the decomposition of either the filler and the aggregate, both calcareous (carbonates based) that chemically decompose at those high temperatures. For temperatures < 100ºC the weight losses detected in the initial SCC are due to the evaporation of the free water, which is not detected in the samples exposed to higher temperatures. The weight losses recorded between 100-350ºC are associated to the dehydration of the cement paste, mainly CSH, which after 300ºC has practically disappeared. The weight losses taking place in the region of 350-500ºC are due to the decomposition of the portlandite. The sample exposed at 1200ºC shows that all the components of the concrete have been altered and no more transformations take place.

The polypropylene fiber shows a melting point at 133ºC and combustion (evaporation) at 444ºC, as determined from TG/DTA given in *Fig.1-right.* This ability of the PPF to melt at relatively low temperatures, would affect the transport process of vapour released from the dehydration of the concrete.

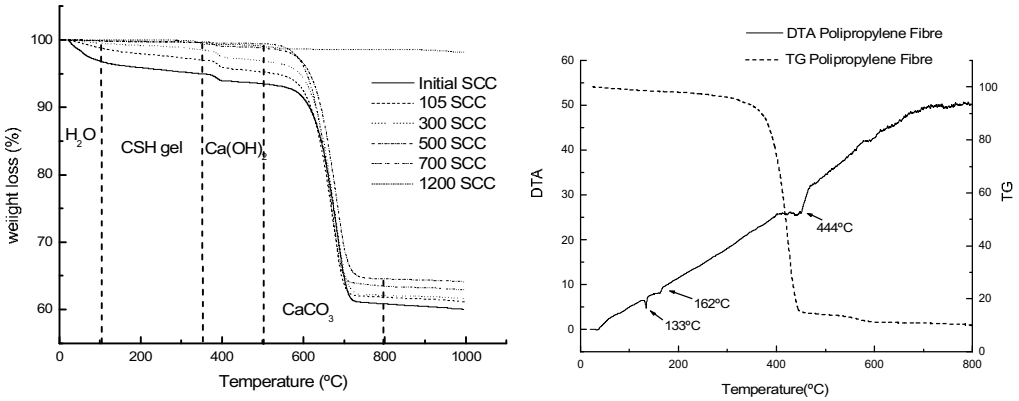

Fig. 1. TG of SCC after high temperature (left). DTA/TG of PPF (right).

Table 1. % of weight loss in different ranges of temperature

Temperatrue	100-350ºC	350-500ºC	500-800ºC
Initial SCC	1.98	1.74	32.02
105 SCC	1.81	1.79	33.41
200 SCC	1.20	1.85	34.95
300 SCC	0.97	1.71	34.66
500 SCC	-	-	35.24
700 SCC	-	-	35.90
1200 SCC	-	-	0.52

2.2 Pore structure changes in SCC with fibers after exposure to high temperature

The pore structure of the SCC concretes undergoes a progressive increase due to heat action, associated with the dehydration of the cement paste components and thermal stresses in the paste, aggregates, filler and PPF, creating open pores, microcracks and empty spaces, as shown in *Fig. 2*. No differences are detected with respect SF, but some curious behaviour is observed in the case of SCC+PPF.

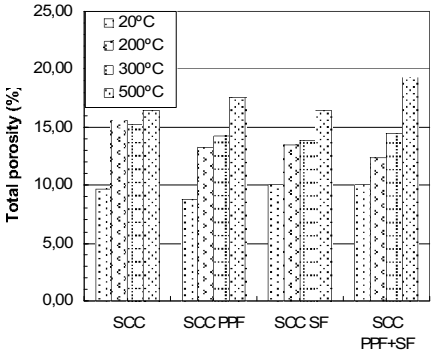

Fig. 2. Total porosity at different temperatures

Small pores, <0.01μm, decrease more intensively in SCC+PPF than for the plain SCC, which no necessarily represents an increase in creation of pores of higher capillary size, the reason is associated to the fact that the melted PPF, occurring 133ºC, might disuse into the small pores

of the surrounding concrete that do no produce the expected increase of porosity, as shown in *Fig. 3, left and right*. The efficiency of the PPF to create more open capillary pores is not noticed until the melted PPF evaporate, which does no occur until 444ºC, present behaviour confirms the previously found by [10, 14].

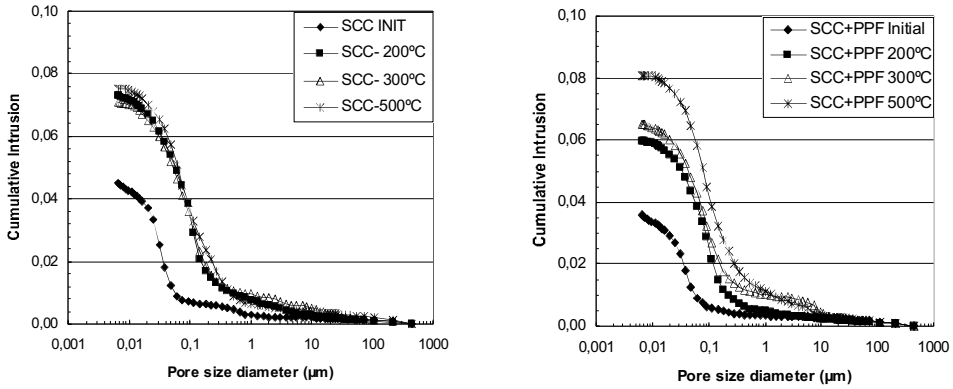

Fig. 3. Pore structure size distribution of plain SCC and SCC+PPF after high T[a]

2.3 Influence of fibers in mechanical properties of SCC under fire

The loss in compressive and indirect tensile strength after exposure to 20, 300, 500 and 700ºC are given in *Fig. 4 left and right*. The presence of fibres seems not to affect the compressive strength evolution, no important differences in compressive strength losses between SCC with and without fibers is determined. However tensile strength decreases more quickly in SCC+PPF than in the others, this fact is attributed first to the PPF loss their beneficial effect in the tensile strength properties after melting; later at higher temperatures after evaporation of the melted fiber creates empty spaces that behave as defects in the concrete. On the contrary the SCC+SF maintain the tensile strength in a higher level up to higher temperatures. At 700ºC the steel fiber is chemically altered (oxidised). The most beneficial in tensile strength at T[a]> 300ºC is the cocktail of fibers: the SF are beneficial due to their better fire resistance which maintain the interaction with concrete, the PPF contribute to open porosity spaces. At 700ºC the behaviour is very similar in all SCC, with and without fibers as both the PPF and the SF have been altered at that temperature.

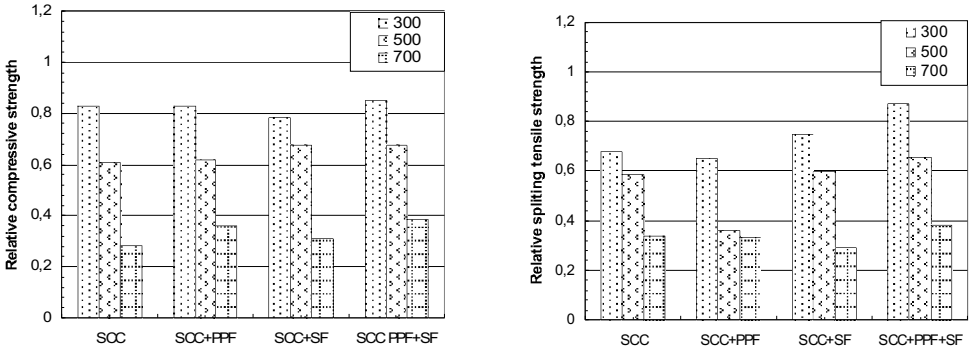

Fig. 4. Relative compressive strength (left) and Relative indirect tensile strength at different temperatures after cooling

2.4 Microstructure changes. Microscopy

When analysing the microstructure of a SCC exposed to high temperature, the progressive loss of density in the material is detected due to the dehydration of the cement paste phases. The main difference observed is in the limestone filler, which loss easily the interaction with the cement paste, as observed in *Fig. 5-left*. Other significant change is related to the presence of the fiber, in particular the PPF, at temperatures bellow 300ºC when the fiber is melted and penetrates into the pores of the surrounding concrete, as observed in *Fig 5-right*.

This response of PPF at high temperatures is important because it is believed that the use of PPF in concrete avoids the risk of explosion under fire due to their ability to melt at the temperature where the risk of explosion is higher up to 300ºC [6, 11, 12] due to the increase of empty spaces leaved by the heat decomposition of the fibers, which relax the high pore pressures generated during heating from dehydration of cement paste. However, recent studies have demonstrated that the risk of spalling due to vapour released still remains even in presence of PPF; the reason can be attributed to the close of pores at temperatures lower than 200-300ºC that not always can be compensated by an increase in pore size due to dehydration of cement paste, so the beneficial effect of PPF in concrete at high temperatures with respect to spalling would also depend on the pore size distribution of concrete, adequate content of polypropylene fibers and w/c ratio of concrete, or the use of PPF fibers with lower range of temperature between melting and evaporation**.**

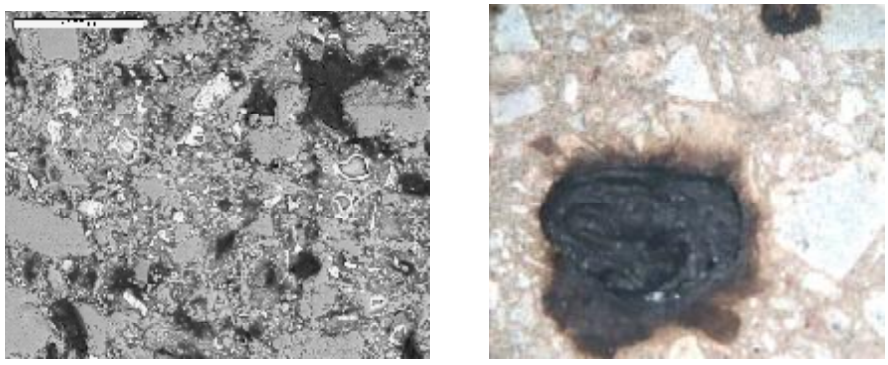

Fig. 5. Left, Backscattered electron microscopy of SCC at 700ºC, x 350. Right, Melting and diffusion of PPF after 300ºC.

3 CONCLUSIONS

- SCC follows similar transformations in microstructure and mechanical properties than plain concrete except that of the filler.
- The changes in pore structure of SCC+PPF suggest close of capillary porosity after the fusion of the fiber, that does no significantly increase until combustion has occurred.
- Mechanical properties of SCC + PPF show higher losses of strain strength.
- SCC +SF contribute to confine dehydrated paste and to control crack developing, until oxidized at Tª above 500ºC.
- SCC with mix of PPF+S F can contribute better to improve the resistance of concrete to fire.

4 ACKNOWLEDGMENT

The authors acknowledge the funding received from the Spanish Ministry of Education and Science PSE-380000-2006-4 / PSE-380000-200681, HABITAT 2030.

REFERENCES

[1] Z.P. Bazant and M.F. Kaplan. Concrete at high temperatures: Material properties and mathematical models. Logman Grp. Ltd., England (1996)

[2] Alonso, C., Fernandez-Municio, L.. Int. WS on Fire Design of concrete structures- From materials modelling to structural performance, Univ. of Coimbra, Portugal, (2007) 69-78.

[3] Fib Bul. nº 38, Fire design of concrete structures, materials structures and modelling. (2007)

[4] Schneider, U., RILEM Int. WS on Durability of high performance concrete. Edt. H. Sommer, Vienna Feb (1994) 237-242.

[5] Ye G., Liu X., De Schutter, Taerwe L., Vanndevelde P.. *Cement and Concrete Research*, 37, (2007) 978-987.

[6] Jansson, R. and Boström, L. Int. WS on fire design of concrete structures from materials modelling to structural performance. *Univ. of Coimbra, Portugal. (2007*) 177-188.

[7] Persson, B. Self-Compacting concrete at fire temperatures TVBM-3110, Lund Institute of Technology. Lund Univ, Division of Building Materials (2003).

[8] Persson, B*, Cement and Concrete Research*, 31, (2001)193-198.

[9] Alonso, C., Andrade, C., Gallo, E. and Menendez, E. 2005. ACI International, SP-229(2005) 289-302.

[10] Kalifa, P. Chéne, G. and Cálle, C. *Cement and Concrete Research*, 31, 10, (2001) 1487-1499.

[11] Khoury, G.A., Majorana, C., Int. WS on fire design of concrete structures from materials modelling to structural performance. Univ. of Coimbra, Portugal. (2007) 211-224.

[12] Suhaendi, S. and Horiguchi,T. Int. WS on design of concrete structures from materials modelling to structural performance. Univ. of Coimbra, Portugal. (2007) 189-197.

[13] György, L. Balázs, Éva, L. 8thInternational Symposium on Utilization of High-Strength and High-Performance Concrete. Nagoya, Japan, 2008.

[14] Alonso, C., Andrade, C., Gallo, E. and Menendez, E., ACI International, SP-229(2005) (2005) 289-302.

[15] Alonso, M.C., Sanchez, M., Rodriguez, C. and Barragan, B., 11th Int inorganic bonded fiber composite conference, Madrid, Nov, 2008.

VARIANCES OF STEEL STRENGHT CHARACTERISTCS IN FIRE TEMPERATURES

Tomasz Domański

Cracow University of Technology,Faculty of Civil Engineering .Krakow,Poland

INTRODUCTION

Laboratory tests provide the only practicable basis for specifying safety margin for ultimate strength of structural members in fire. The reliable safety measure in design of steel member in fire is probability of failure $p_f = P(Ex,Ex^2;t)$. The probability function $P(Ex,Ex^2;t)$ depends on two parameters :expected value Ex of strength in temperature t (mean or median value) and variation parameter Ex^2 (variance or coefficient of variation).The relationship between expected value of strength (mean, median value) and temperature is well known but relations between variation parameters (variance, coefficient of variations) are still taken into consideration. In this paper ,the results of laboratory tests of strength characteristics in fire temperatures for two kinds of steel (F 230JR,F350JR) and for two kinds of shapes are presented. The basic question which ought to be stated is which variation parameters (variance or coefficient of variation) are constant in fire temperatures to create probability function of strength characteristics and consequently probability function of failure in fire temperatures . Then ,it is necessary to test two equivalent hypothesis :H_0 : variance is constant versus H_1 : coefficient of variation is constant in fire temperatures. The analysis of variance in two – way hierarchical classification case was applied to estimate variance from fixed effects of different kinds of steel and shapes. The Bartlett's statistic B to verify hypothesis H_0 and H_1 which is asymptotically convergent to chi-squared distribution was applied.

The results of these investigations make possible to create probability function of fire resistance which is essential to estimate fire safety of steel structure

1 DESIGN CONDITIONS

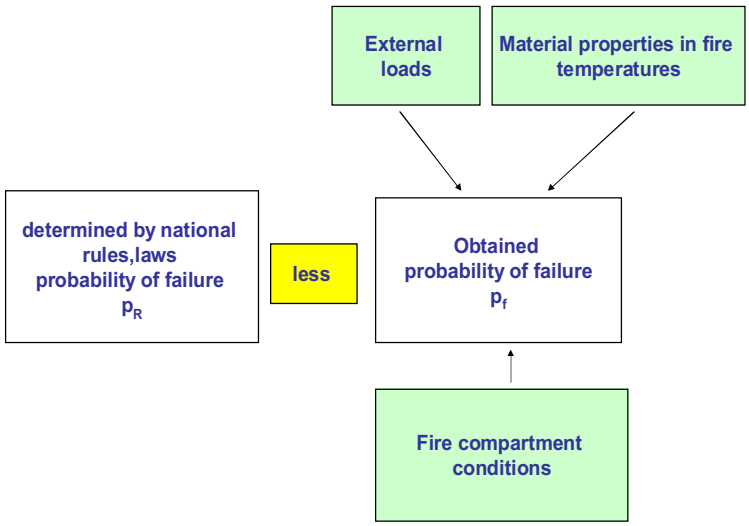

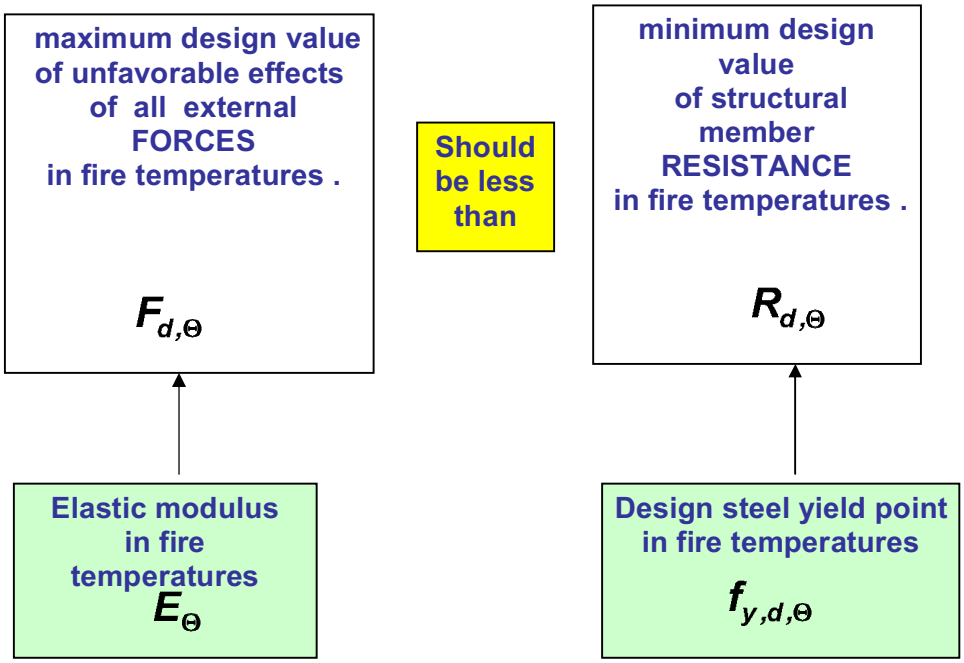

It is assumed that structural member could support external and accidental fire forces according to EN 1991-1-1 , repeated in particular standard EN 1993-1-2 [5],[6],[7] as follows:

$$F_{d,\Theta} \le R_{d,\Theta} \quad . \tag{1}$$

Where : $F_{d,\Theta}$ is the maximum design value of unfavorable effects of all the external force combinations in fire temperature Θ.
$R_{d,\Theta}$ is the minimum design value of structural member resistance in fire temperature Θ.

1.1 Design value of steel yield point in fire temperatures

The yield point $f_{y,k}$ decreases when fire temperatures Θ are grown ,then

$$f_{y,k,\Theta} = k_{y,\Theta} f_{y,k,20}, \quad f_{y,k,20} = \breve{f}_y \exp(-1.64\nu_{fy,20} - 0.5\nu_{fy,20}^{\,2}). \tag{2}$$

Where; $\breve{f}_y, \nu_{fy,20}$ are the median and log-normal coefficient of variation of the steel yield point in temperature $\Theta = 20^oC$.
It has been assumed that applied value of characteristic strength $f_{y,k,20}$ is described in normal – room temperature $\Theta = 20^oC$.The reduction coefficient $k_{y,\Theta}$ for different fire temperatures Θ is presented in standard EN 1993-1-2.This relation is described as:

$$R_{k,\Theta} = k_{y,\Theta} R_{k,20}$$

Constant value of $\gamma_{M,fi}$ in fire duration (particularly $\gamma_{M,fi}$=1) provides to the following formula for design value of the steel yield point in fire temperature Θ.

$$f_{y,d,\Theta} = \frac{f_{y,k,\Theta}}{\gamma_{M,fi}} = \frac{k_{y,\Theta} f_{y,k,20}}{\gamma_{M,fi}} = k_{y,\Theta} f_{y,d,20} \qquad f_{y,d,20} = \breve{f}_y \, exp(-3.04\nu_{fy,20} - 0.5\nu_{fy,20}{}^2), \qquad (3)$$

and also for design resistance

$$R_{d,t,\Theta} = R_{d,t}(\Theta_a) = k_{y,\Theta} R_{d,20} \quad . \qquad (4)$$

The R_Θ is the random variable described by log-normal probability distribution function $\mathcal{N}(\breve{R}_\Theta, \nu_R)$ - $\breve{R}_\Theta$ is median value and ν_R is the log-normal coefficient of variation. Reduction coefficient $k_{y,\Theta}$ is defined for different fire temperatures Θ .Temperature Θ will be treated as no-random in this analysis. There is the relation :

$$\breve{R}_\Theta = k_{y,\Theta} \breve{R}_{20} \quad . \qquad (5)$$

It has been assumed that log – normal coefficient of variation ν_R does not depend on temperature Θ ,then:

$$\nu_{R,\Theta} = \nu_{R,20} = const \quad \text{and} \quad \nu_{fy,\Theta} = \nu_{fy,20} = const \qquad (6)$$

The problem of acceptance equality (8) will be taken into consideration in the next part of this paper.

2 VARIATION PARAMETERS – STATISTICAL TESTS IN FIRE TEMPERATURES

2.1 Populations, groups, samples

Let $\underline{Y}_{ijk}$ be the set of measured values of the basic variables (e.g., steel yield point, modulus of elasticity) for a particular test specimen. A set of n identical specimens constitutes a sample from the population of all possible specimens built to the same specified values of $\underline{Y}$. The statistical properties, such as the variances or coefficients of variation of $\underline{Y}$,may be approximated by the variance, coefficient of variation of $\underline{Y}_{ijk}$ from the samples and a calibration for the population will be based on these properties. The samples $\underline{Y}_{ijk}$ were defined for two kinds of steel grades i=1,2(S235JR,S355JR) , for two kinds of steel members j=1,2 (bars, hot rolled sections) and for k=1…4 temperatures (20,300,400,500 ^oC).
The tests were performed for "small-sample size" n=6 estimating yield point $f_{e,\ I,j,k,\nu}$ and $E_{I,j,k,\nu}$ -ν=1...6.The N=96 laboratory data were obtained.

2.2 Outline of used statistical methods – assumptions

- There were different grades and shapes of steel members to get large variance inside samples $\underline{Y}_{ijk}$ taken into the consideration
- The variances from permanent effects (different factors-grades, shapes) for group $\underline{Y}_k = \bigcup_{ij} Y_{ijk}$ for temperatures k=1…4. were obtained. It is supposed that variations

parameters of $\underline{Y}_k$ can be constant, can increase or decrease but can not be non-monotonic in fire temperatures Θ.

- There were two parameters of variations taken into consideration:
  - standard deviation $\sigma_k = (\mathrm{Var}(Y_k))^{1/2}$
  - coefficient of variations $V_k \cong \vartheta_k = (\mathrm{Var}(\ln \underline{Y}_k))^{1/2}$, ϑ_k -log-normal coefficient of variation.
- Analysis of variance was applied to estimate σ_k and V_k to separate gross laboratory errors.Two levels of factor A (steels S235Jr,S355JR r=2)and two levels of factor B(bars,

hot rolled sections s=2)within each levels of factor A were considered. Analysis of variance was applied for laboratory results for each k=1..4 temperatures Θ separately.

2.3 Analysis of variance

2.3.1 Outline of methodology

It was accepted that :formula for "ν" test results $Y_{ij\nu}$ (steel yield point, modulus of elasticity) in temperature Θ(k) separately, for " j" level of factor B within "i" level of factor A [1]:

$$Y_{ij\nu} = \mu + a_i + b_{ij} + e_{ij\nu}. \quad (7)$$

Where: i=1…r , j=1…s , ν=1…6,

μ - mean value in sample $\underline{Y}_{ijk}$

a_i , b_{ij} , $e_{ij\nu}$ – non correlated random variables with expected value equal null and partial variances : var(a_i)=σ_a^2, var(bij)= σ_b^2 ,var($e_{ij\nu}$) = σ_e^2 for all I,j,ν.

Variances σ_a^2, σ_b^2 , σ_e^2 are partial of complete variance in temperatures Θ(k);

$$\sigma^2 = \text{var}(Y_{ij\nu}) = \sigma_a^2 + \sigma_b^2 + \sigma_e^2. \quad (8)$$

The result of permanent effect actions are variances σ_a^2 , σ_b^2 (steel grades and shapes).The problem is to estimate variances from permanent actions σ_k^2 free from laboratory errors:

$$\sigma_{per}^2 = \sigma_a^2 + \sigma_b^2. \quad (9)$$

The estimation of variances σ_a^2 , σ_b^2 , σ_e^2 should be calculated upon classic analysis of variance methods [1] and variance from permanent actions factor – A and B ;

$$\hat{\sigma}_{per}^2 = \hat{\sigma}_a^2 + \hat{\sigma}_b^2 . \quad (10)$$

2.3.2 Influence of factors A and B on variance $\hat{\sigma}_{per}^2$.

It is necessary to test the null hypothesis H_0: $\sigma_{per}^2 \neq 0$ against the alternative hypothesis H_1: the variances are equal ; $\sigma_{per}^2 = 0$ [2].Hypothesis about existing treatment A – H_o is accepted when $MQ_A/MQ_R \leq F_\alpha(f_A,f_R)$ and is rejected when $MQ_A/MQ_R > F_\alpha(f_A,f_R)$,where $F_\alpha(f_A,f_R$ is the critical value of the F-Snedecor distribution with f_A,f_R degrees of freedom. Null hypothesis will be tested at the α level of significance .Alternatively , we test the null hypothesis H_o about existing treatment B .We accept hypothesis H_o when $MQ_B/MQ_R \leq F_\alpha(f_B,f_R)$ and reject it when $MQ_B/MQ_R > F_\alpha(f_B,f_R)$.The variances of two variables (steel yield point ,modulus of elasticity in fire temperatures) and for two statistics : σ = (var (Y))$^{1/2}$ and $V = \sigma_{ln}$=(var (lnY))$^{1/2}$ were analysed .The influences – interactions of factors A and B on variation parameters of yield point ($Y=f_d$) are shown in *Table 1* [3].[4].

*Table 1.*Influence of factors A,B on standard deviation σ of the steel yield point ($Y=f_d$)

Θ [°C]	MQ_A/MQ_R	$F_{0.05}(1,20)$	Interaction A	MQ_B/MQ_R	$F_{0.05}(2,20)$	Interaction B	$\hat{\sigma}_{st}$ (f_y)[Mpa]
20	294.42	4.35	exist	24.24	3.49	exist	76.74
300	49.10	4.35	exist	4.45	3.49	exist	60.92
400	66.68	4.35	exist	2.42	3.49	exist	62.89
500	83.21	4.35	exist	6.30	3.49	exist	42.75

Analysis of above tables gives basis to state existing influence of factor A,B for yield point of steel parameters of variations , that is $\sigma_k(f_y) \neq 0$ and $V_k(f_y) \neq 0$ for any fire temperatures Θ .These thesis cannot be supported for variation parameters of modulus of elasticity E in fire temperatures. Then upon *Table 2* we can state that : $\sigma_k(E) = 0$ and $V_k(E) = 0$

Table 2. Influence of factors A,B on variation parameters of modulus of elasticity E ($Y=E, Y=lnE$)

Θ [°C]	20	300	400	500
MQ_A/MQ_R for $Y=E$	1.75	0.25	0.35	4.15
MQ_A/MQ_R for $Y=lnE$	1.76	0.74	0.496	1.21
$F_{0.05}(1,20)$	4.35	4.35	4.35	4.35
Interaction A,B	no- exist	no- exist	no- exist	no- exist

2.4 Standard deviation σ and coefficient of variation V of the steel yield point in fire temperatures

Now,it is necessary to test hypothesis H_o - equality of variances :$\sigma_k^2 = \text{var}\,(Y_k)$ in fire temperatures. The null hypothesis H_o is : $\sigma_1^2 = \sigma_2^2 = \ldots = \sigma_k^2$ against alternative hypothesis H_1: $\sigma_1^2 \neq \sigma_2^2 \neq \ldots \neq \sigma_k^2$ for all fire temperatures Θ(k) and adequately for $V_k^2 = \sigma_{ln,k}^2$ the null hypothesis H_o: $\sigma_{ln,1}^2 = \sigma_{ln,2}^2 = \ldots = \sigma_{ln,k}^2$ against alternative hypothesis H_1: $\sigma_{ln1}^2 \neq \sigma_{ln2}^2 \neq \ldots \neq \sigma_{lnk}^2$ .Above hypothesis will be verified by using Bartlett's test which is supported upon following statistic[2]:

$$b = \frac{\left(\prod_{i=1}^{k} \sigma_i^2\right)^{n/(N-k)}}{\sigma_p^2} , \qquad (11)$$

where: n- sample quantity , $n=24$, $i=1 \ldots k=4$, $N = k\,n = 96$,

$$\sigma_p^2 = n \sum_{i=1}^{k} \sigma_i^2 / (N-k) \qquad (12)$$

We accept hypothesis H_0 at the α level of significance when :$b < b_k(\alpha;n)$
$b_k(\alpha;n)$ – critical value for Bartlett's test ,k –number of populations in fire temperatures , α – level of significance ,n – sample quantity.
The Bartlett's statistic b_{fe} to verify hypothesis about equality of yield point standard deviation in fire temperatures $\sigma_1^2 = \sigma_2^2 = \ldots = \sigma_k^2$ was estimated as follows;

$$b_{fe} = 1.171 > b_4(0.01\ ,\ 24) = 0.882 \qquad (13)$$

then hypothesis H_0 ($\sigma_1^2 = \sigma_2^2 = \ldots. = \sigma_k^2$) is rejected, σ_k^2 - variance of the steel yield point in fire temperature.
Consistently ,the Bartlett's statistic b_{lnfe} to verify hypothesis about equality of yield point coefficient of variations in fire temperatures $V_1^2 = V_2^2 = \ldots = V_k^2$ was estimated ;

$$b_{lnfe}\ 0.247 < b_4(0.01\ ,\ 24) = 0.882. \qquad (14)$$

In this case we accept hypothesis $H_{0:}$ $V_1^2 = V_2^2 = \ldots = V_k^2 = const$ and $\nu_{fy,\Theta} = \nu_{fy,20} = const$.

V_k^2 – coefficient of variation of the steel yield point in fire temperatures.

3 SUMMARY

- It can be assumed at the α level of significance that the variations parameters of the steel modulus of elasticity E in fire temperatures is equal null.
- The variations parameters of the steel yield point (coefficient of variations, variance) in fire temperatures are significant and are not equal null.
- For reasons given above the coefficient of variation of the steel yield point is constant in fire temperatures
- More research is needed on the coefficients of variations ,as found in practice, of some of the basic variables, and on the assumption that the distribution of the steel yield point in fire temperatures is log-normal.

.

REFERENCES

[1] Dunn O.J., Clark V.A., Applied Statistic: Analysis of Variance and Regression, *John Willey Sons* N.J.,1987

[2] Walpole R.E., Myers R.H., Myers S.L., Probability & Statistics for Engineers & Scientists, *Prentice Hall.*N.J.2002

[3] Domański T., Variation Parameters of Structural Steel, Characteristics in Fire Temperatures. *Eurosteel 2008, 5th Conference on Steel and Composite Structures,2008 Graz, Austria. Publishing by ECCS,1200 Bruseels, Belgium.*

[4] Maślak M., Domański T., Safety factors in design of steel members for accidental fire situation. In: *Proc. of the DFE2008 Int. Conf. "Design ,Fabrication and Economy of Welded Structures .Miskolc. Horwood Publishing Ltd.London,*2008.

[5] EN 1990: Eurocode –Basis of Structural Design.

[6] EN 1991-1-2:Eurocode 1:Actions on Structures – part 1-2:General Actions-Actions on Structures Exposed to Fire.

[7] EN 1993-1-2:Eurocode 3:Design of Steel Structures – Part 1-2:General rules – Structural Fire Design.

Application of Structural Fire Engineering, 19-20 February 2009, Prague, Czech Republic

FIRE DAMAGE OF STONE STRUCTURES

Mónika Hajpál

ÉMI – Non-profit Company for Quality Control and Innovation in Building, Budapest, Hungary

INTRODUCTION

Nowadays mostly the historic buildings are built of stone, they have also stone structural elements, the modern buildings contains only stone parts (embellishment, floor-plate). Natural stones were frequently used as building material in our historical monuments due to their advantageous properties. The finely carvable and well workable ones were applied as raw material of trim-stones, frontal ornamentations or sculptures. The hard, compact types were exceedingly applicable for load-bearing, structural elements (cope, vault, column, pillar, stairs, access balcony, lintel, bracket, etc.). The most popular types were able to be used both ways. Stone buildings were damaged by fire from ancient times until quite recently. In the stone material the fire causes irreversible changes, which influence the strength and static behaviour of the whole monument.
Some fires at the end of 20th century brought attention to the severe damage that fires can cause to historic buildings and their building stones.
There are some example mentioned without requiring completeness for historic fire incidents, which are well known since they were published in the world press:

- York Minster (1984)
- Hampton Court Palace (1986)
- Chiado, Lisbon, Portugal (1988)
- Uppark House, England (1989)
- Katarina Church, Stockholm Sweden (1990)
- Windsor Castle, England (1992)
- Odd Fellow Palace, Copenhagen (1992)
- St. Michaels Church in Newquay (1993)
- Redoutensal, Hofburg Palace, Vienna, Austria (1992)
- Theatre “La Fenice”, Venezia (1996)
- Cathedral of Torino “Sacra Sindone”, Torino (1997)
- St. Michael Church, Budapest (1998)

Till the 1990s mostly only fire resistance of wood, steel and concrete have been investigated. Due to prefabricated buildings the studies have been limited to the role of stone as an aggregate for concrete. Previous researches on the effects of fire on monumental stones have mainly focussed on morphological changes taking place on stone surfaces such as cracking, scaling [1, 2] or analyses of colour changes [3]. A few mechanical properties of fire-damaged sandstones or heated specimens were also measured [4, 5, 6]. Previously few researcher [7, 8, 9] have shown that sandstones are sensitive to heat by oven tests under laboratory conditions. They provide valuable information on the thermal behaviour of sandstones, the mineralogical and textural changes have been also published in detail.
In this paper first the traces of deterioration by fire are shown, then the results of petrological and petrophysical laboratory tests made on different stone type samples are demonstrated. The futural research will focus on the statical analysis of fire damaged stone structures. A computer model will be used for analyzing the statical behaviour and load carrying capacity of structural part simultaneously subjected to normal loading and high temperature.

1 DECAYS, TRACE OF FORMER FIRES

The measure of damage caused by fire depends on many factors. The changes at the natural stones could be influenced by the burning circumstances, e.g. is the heating one-sided or more-sided, homogenous or heterogeneous, the size of the burned stone, velocity of heating, the maximum burning temperature, stone type and its characteristics.

The one-sided and quick heating is much more disadvantageous. Thin elements like plates become warm sooner and thus are suffering less than the blocks. Fires can be small and localized, which generally do not generate much heat and their damaging effect is limited to surface effects and soiling of the surface by smoke. On the other hand the large and widespread fire generates more heat and as a result it has a significant effect on the physical-chemical properties of stone structure. The maximum temperature is 800°C in case of small fires, by large-scale catastrophic fires some hundred degrees more, but by burning significant amount of inflammable materials could cause much higher burning temperature.
The decay is a form of physical and chemical changes in stone. The changing of the rock constituent minerals and the inner structure induce the character and degree of the decay on effect of heat.
The **colour changes** in natural stones almost corresponds to the dehydration of iron compounds. Heat causes the development of a pink or reddish-brown colouration in brown or buff-colour (Fig.1.). It does not occur among white or grayish stones, which are relatively free from iron oxide. The colour changes start at a temperature of 200-300°C in most rocks and it may not be apparent until a somewhat higher temperature. By testing of big stoneblocks is a sharp boundary between the heated, red-coloured stone surface and the unaltered stone behind. These zone has a width about 2-3 cm or less. Some stones contain a small amount of organic substance which cannot be seen and which is seldom found in analysis. At about 500°C this organic matter begins to turn into coal and effects a grey colour covering the red one. At an increased temperature the carbon is burnt away and the original colour is visible again.

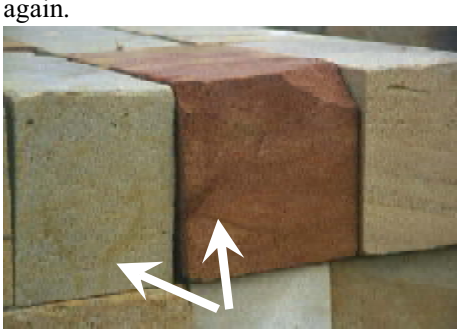

Fig. 1. Colour changing

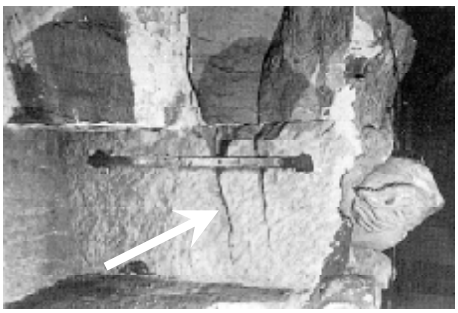

Fig. 2. Cracking

Other significant kinds of decay of stones by burning are cracking (Fig.2.), shattering, scaling, spalling, which completely destroy the richer carved forms of architecture and damages the smoother forms. They are often so badly spoiled that they have to be replaced by new ones.
Heat effect related **spalling** of sandstone is to seen on Fig.3. At this window of the Monastery in Lobenfeld, in Germany the stone was quickly heated from one side, but it was still cold in its inner parts. The process of scaling is continued during the fire, therefore the strength of the stone is surpassed and a bursting of the hot outer part is forced and the rock peels like an onion. In the simplest cases the bursting of occurs in shells parallel to the surface: a sphere will burst in spherical calottes, a column in cylindrical shells.
Rounding off the edges can occur if there is an edge the heat can work from two sides. This form of decay is regularly seen on steps, edges of pillars and window-heads. Fig.4. shows a rounding of edges by fire a sandstone column at the Heidelberg Castle (Germany).
Breaking is typical where single parts are jutting out of a plane (Fig.5.). It heat up more quickly and burst off easier, since the stresses find the way out more quickly (e.g. scaling of bosses just to the depth of groove, the bursting of the ribs of channelled columns, etc.).
If the jutting part is sharply divided from its neighbourhood often arise additional notch effects. All kinds of carving in stones will influence the form of bursting. At a very long

heated construction (e.g. a door post or the longstep of a staircase) a distribution of the stress is not effected across the whole length, the length will be subdivided by means of small transverse cracks into divisions which will scale separately and the result will be a range of pillow-formed surfaces [2, 8].

Fig. 3. Spalling

Fig. 4. Rounding edges

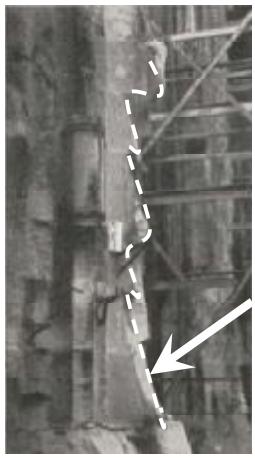

Fig. 5. Breaking

The texture will heavily influence the form of decay by inhomogeneous stones. Layers of mica, lamination, other cleavage planes or fine capillary cracks are always spots of failure and they will burst off at any rate. In stone structures tensions are by means of heating, differential dilation, and also from payloads and deadloads. In highly loaded pillars the exterior parts can be already overloaded and the additional heat stresses may cause disintegration. It is very important that we don't have to know only the behaviour of building stones, but we have to face the whole construction.

2 MATERIAL PROPERTIES

Hungarian stone types frequently used in historical monuments were taken into the experiments. Three types of sandstone, three types of limestone and a rhyolite tuff were chosen for the investigation. Besides I applied in my research seven types of German sandstones, and in cooperation with other researcher Portuguese and Spanish stones are also examined. The selected stone types showed a wide range of their feature (colour, grain size, cement type, age, rock constituent minerals, porosity, strength). This compositional variation enables us to achieve a better understanding of how such properties influence the behaviour of natural stones under heat.

Three types of Hungarian sandstones were used for the thermal tests: Balatonrendesi, Ezüsthegyi and Rezi. Seven German sandstone types were also investigated. The analysed quartz sandstones have different characteristics (grain size, porosity). The mineralogy of cements and the colour also varies [6, 8]. The three types of limestones (Tardos compact limestone, Süttő travertine, Sóskút oolitic limestone), which were used for the thermal tests represent the most widely used monumental stones in Hungary [10]. The creamy colour rhyolite tuff from Egertihamér is used as ashlars in one of the most visited historic site of North-Hungary, in the Eger Castle and in environs.

3 INVESTIGATION METHODS

Because of the complexity of the processes taken place in case of fire and the lack of knowledge of the behaviour of stone material a simplified heating method was used for the simulation of the effect of fire. From the stone blocks cylindrical specimens (40 mm in

diameter and 40 mm to 80 mm in height) were prepared. The specimens were heated in an oven at 6 different temperatures (150, 300, 450, 600, 750, 900°C) for 6 hours. Warming up took 1 hour, and after controlled heating the specimens cooled down slowly in the oven. The samples were tested before and after the heating processes carried out at each temperature.
The mineralogical composition of the samples heated to the different temperatures was determined by X-ray powder diffraction (XRD: Siemens D500) and by differential thermal analyses (DTA: MOM Derivatograph, 20-1000°C). Textural and mineralogical alterations were visualized under polarizing microscope in thin sections and by scanning electron microscopy (Cambridge Stereoscan). The petrophysical analyses included the measuring of specific and bulk density, porosity, water adsorption, duroskop hardness, ultrasonic sound velocity. Indirect tensile strength test and uniaxial compressive tests were also made. The colour changes were tested with CIELAB method.

4 RESULTS

4.1 Mineralogical analyses

As result of the mineralogical analyses the changes of the texture and inner structure and hereby the increasing in porosity, the disappearance of minerals or formation of new mineral phases and the colour change are observable. On effect of heating the quartz and K-feldspar do not show significant alteration up to 900°C. As major effects the transformation of α-quartz to β-quartz (580-595°C) and the formation of micro-cracks at quartz and feldspar grain boundaries above the 600°C heating temperature were detectable. Micro-cracks develop also within the crystals but only at higher temperatures (above 750°C). Clay minerals and phyllosilicates show several transformations on heat effect. In the ferruginous sandstone (Balatonrendes) the changing of the iron-hydroxide and the kaolinite was shown. The micas iron contents oxidize and the clayey cement comes away from the pore wall in Ezüsthegy sandstone and hereby the mineral become dark. The structure of kaolinite mineral partly collapse after 750°C the, but thanks to the extremely large crystal size it is recognizable yet. Illite-smectite structures are more stable than kaolinite, it can be still detected at 900°C, although at 553°C it looses it hydroxyl radicals. The jarosite mineral in the Rezi sandstone changed its colour to yellowish brown by heating and it modified to hematite above 450°C. Kaolinite and chlorite first coloured by increasing the temperature then ruined additionally in the inner structure and in quartz grains cracks occurred. Due to calcination processes at limestones in the carbonate minerals the major changes took place at 450°C and above. At 750°C the structure of calcite collapsed and at 900°C calcite and dolomite was not possible to detect; however after leaving the samples at room temperature for two hours at about 45% relative humidity a new mineral phase, portlandite was detected. This is a reaction product of air humidity (water) and CaO and associated with a volume increase of 20% in average and leads to the disintegration of cylindrical specimens. In Tardos limestone a thin film of iron oxides cover the calcite crystals in some places and this degrades with the heating. In the Süttő travertine the calcite crystals are very rough, which show that the deposition was very quick. Thermal cleavage, inter-granular crackings and incipient surface dissolution of grains occurred at the effect of heat. In Sóskút coarse limestone the heating makes small inter- and intragranular cracks arisen, which occur decided porosity increasing at elevated temperature. In Egertihamér rhyolite tuff bentonite flakes cover the surface of lithic clasts as a thin film. Above 750ºC this is not yet recognizable.

4.2 Petrophysical investigations

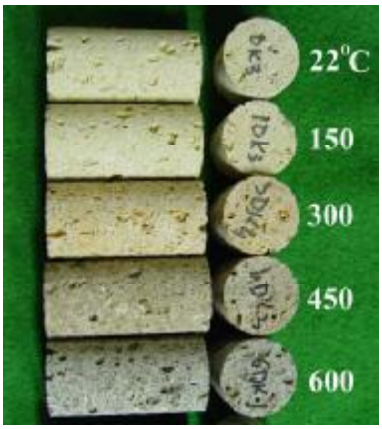

Fig. 6. Colour changing by Sóskút coarse limestone samples

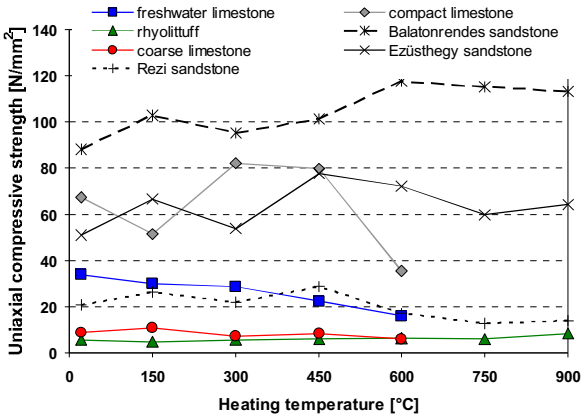

Fig. 7. Uniaxial compressive strength values as function of heating temperature at different stone types

The limestone samples were sensitive at the heating. On the compact limestones specimens small hairline cracks arised already after at heating on 450°C and over the 600°C heating temperature the samples exploded. These specimens faded at the elevated temperature (750°C). The travertine samples grown dark till 450°C and smelt foul due to organic matter content, but after this there also paled. These specimens survived the heating, but some hours after the test the CaO had reaction with the air moisture and due to nascent portlandite and the volume increment the samples crumbled. The coarse limestone samples also stand out the effect of heat at 750°C and 900°C, but they have falled into dust soon (Fig. 6). Some reports [3, 7] mention this process by high temperature tests of calcite containing stones. The heating did not result similar problems at the sandstones and the rhyolite tuff samples.

The colour changing was detectable by eyes (Fig. 6), but for the correct determination instrumental testing was (CIELAB method) also used. The colour modification of stone types was different. The dark grey colour of travertine samples at elevated temperature and the nascent hum indicates to organic matter content. Fig. 7 shows the results of the compressive strength test as function the heating temperature. It can be observed, that the heating does dot causes a decrease in the strength in all cases. The Balatonrendes and Ezüsthegy sandstone and also the Egertihamér rhyolite tuff has higher strength after the heating at 900°C as in the beginning state before heating. The limestone types lost their strength not promptly but only at elevated temperature.

5 SUMMARY

At the effect of heat changes take place in the inner structure and mineral composition of the natural stones, which influences the petrophysical parameters (porosity, strength, water adsorption, colour). This changing is not always adverse, but we have to take it to account for instance at the restoration of a fire damaged stone building. The mineralogical composition and texture of natural stones significantly influence their resistance to fire and the thermal changes. The heat resistance of different quartz sandstone depends on the type of the cementing mineral, the amount of cement (grain/cement ratio), the grain size (fine, medium, coarse) and the grain to grain or matrix to grain contacts. The initial porosity, compactness influences the behaviour of limestone and rhyolite tuff at heat effect. The compact stones show more dramatic change in porosity at elevated temperatures than the less cemented ones and they are more rigid. At a porous and cement rich stone is more adaptable, these can adopt

the addition strength caused by thermal expansion. The mineral composition is also determinant factor. The silica cemented, ferruginous or clayey stones are less sensitive than the carbonatic ones, which disintegrate at higher temperature. It is to be regretted that it is not possible to use the sequence of colours as a scale of temperature. The amount of colouring substances is different with every square stone, and one can see the most varied degrees of colours on a heated wall. The degree of temperature and the duration of heating can replace each other to a large extent.
In the future the results of petrological and petrophysical laboratory tests can help as input at the calculation by fire damaged stone structure. This kind of computer model will be used for statical analyzing the statical behaviour and load carrying capacity of structural part simultaneously subjected to normal loading and high temperature.

6 ACKNOWLEDGMENT

The author gratefully acknowledges the support of her earlier workplace the Budapest University of Technology and Economics (BUTE), Department of Building Energetics and Building Services, Laboratory of Building Physics and her supervisor, Dr. Ákos Török (BUTE, Department of Construction Materials and Engineering Geology) for his valuable help during the research work in the last years.

REFERENCES

[1] Kieslinger A., Zerstörungen an Steinbauten, Franz Deuticke. Leipzig und Wien, 1932

[2] BRE, Repair of Damaged Buildings—the repair of stonework damaged by fire. *Garston Building Research Establishment Note 21:1–5,* 1945

[3] Chakrabarti B., Yates T., Lewry A., Effect of fire damage on natural stonework in buildings. *Construction and Building Materials (10)*, pp. 539–544, 1996

[4] Chakrabarti B., An assessment of effects of fire damage to stone in buildings & procedures for restoration and conservation of stone in some historic stone buildings. *Building Research Establishment Note 93(15),* pp 2–14, 1993

[5] Allison RJ, Goudie AS, The effects of fire on rock weathering: an experimental study. In: Robinson DA, Williams RBG (eds) *Rock Weathering and Landform Evolution. Wiley*, Chichester, pp 41–56, 1994

[6] Hajpál M, Török Á., Mineralogical and colour changes of quartz sandstones by heat. *Environmental Geology, 46 (3-4)*, pp. 311-322, 2004

[7] Török Á., Hajpál M., Effect of Temperature Changes on the Mineralogy and Physical properties of Sandstones. A Laboratory Study. *International Journal for Restoration of Buildings and Monuments, 11 (4),* Freiburg, pp. 211-217, 2005

[8] Hajpál M., Changes in sandstones of historical monuments exposed to fire or high temperature. *Fire Technology 38(4)*, pp. 373–382, 2002

[9] Hajpal M., The behaviour of natural building stones by heat. *Fracture and Failure of Natural Building Stones. Applications in the Restoration of Ancient Monuments*, pp. 439-445, 2006

[10] Gomez-Heras M., Alvarez de Buego M., Fort, R, Hajpál, M., Török Á., Varas M.J., Evolution of porosity in Hungarian building stones after simulated burning. In: Fort, R, Alvarez de Buego M., Gomez-Heras M. & Vazquez-Calvo C. (Eds): *Heritage Weathering and Conservation, Taylor & Francis/Balkema, London. Vol. I*, 513-519, 2006

THERMAL CHARACTERISTICS MEASUREMENTS OF AN INORGANIC INTUMESCENT COATING SYSTEM

J. Yoon Choi, Hyun Min Jang, Chaemin Chun [a]

[a] Korea Institue of Construction Materials, Weathering Technology Center, Seoul, Korea

1 INTRODUCTION

Intumescent coatings are widely used to improve thermal resistance of steel building structures under fire conditions. By knowing the thermal characteristics of an applied intumescent coating system as a function of temperature, the insulating properties of intumescent coating protected steel structure could be better understood.

However, intumescent coatings, as their nature, exhibit time and temperature dependant changes of physical and chemical properties when they are exposed at thermal sources. These time and temperature dependant properties include thermal diffusivity, density and specific heat capacity etc. These would be some of the important values to be used for the prediction of structural safety under fire conditions.

Substantial amount of commercially available intumescent coating systems are comprised of polymer resin with ingredients such as intumescent agents, fillers and property enhancers. In depth polymer resin contained intumescent system has been investigated [1-3]. Although advantageous aspects, which would include harder expanded insulating layer and low gas evolution during expansion, can be achieved by excluding polymer resin, a few intumescent systems exclude polymer resin as the continuous medium [4] [5].

A commercially available inorganic intumescent coating system, of which applicability as a passive fire protection product under ISO 834 fire test condition is reported, was chosen and physical and chemical changes were measured and reported in this paper.

2 EXPERIMENTAL

A commercially available inorganic intumescent coating product named FC-MAX [6], which is a water dispersion of inorganic particles, was used for this work. Reported main ingredients include sodium silicate as the expanding agent, titanium dioxide and aluminium oxide as fillers and Kaolinite as the substitute of polymer resin.

Intumescent coating samples were prepared using an automatic film applicator, PA2101 Byk Gardner, to achieve uniform sample thickness of wet coated film, and then the film was dried under room condition until no further weight decrease was measured. The dried samples were used here after experiments unless otherwise specified. For heat treatment, samples were located within an electric oven that was set up at wanted temperature for 30 minutes.

Images of samples were acquired using a HITACHI S-3000H SEM. To characterize time and temperature dependent behaviours of the interested sample, NETZCH STA 409PC, QMS 403C STA-MS was used between room temperature and 1400℃ at elevating temperature

speed of 10℃/min. Under the same test conditions NETZCH STA 409PC was used to analyze the weight changes. To characterize evolving gases during the heating period MS was used simultaneously. Specific heat capacity measurements were performed using NETZCH DSC 404 to increase accuracy at higher temperature ranges. Also these samples were used to measure thermal diffusivities using a laser flash apparatus, NETZCH LFA 457

3 RESULTS AND DISCUSSION

Intumescent coating solution was diluted with water then particles within the solution were collected with a filter paper. Surface image of the collected particles is presented at Figure 1. The image indicates the particle size of the ingredients of the dried coating is within the order of um. Hexagonal flake shape particles shown at the figure represent Kaolinite. This image would indicate that lab scale thermal experiments including DSC, TG, MS and LFA that only use mg scale samples would be sufficient enough to represent the whole system. Figure 2 shows the intumescent system after expansion at 600℃.

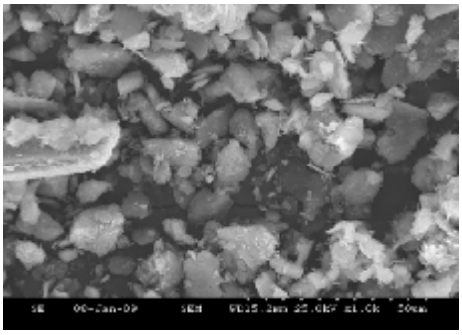

Fig. 1. SEM image of ingredient particles

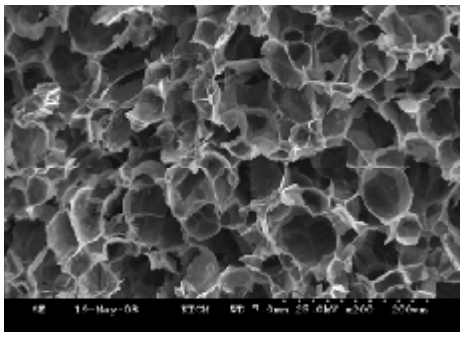

Fig. 2. Expanded intumescent coating at 600℃

To analyze thermal reactivity of the system, DSC and TG were applied and the result is shown at Figure 3. This indicates that endothermic reaction appears between ca 118.8℃ and 168.2℃. During this period approximately 9.2% w/w mass decrease was measured. At this temperature range inflation of the sample i.e., intumescent characteristics could be observed as well. As was reported sodium silicate and Kaolinite lose absorbed water around 100 ℃ and the process ends at 200℃ [7], [8]. For the case of Kaolinite, dehydration process of physically adsorbed water goes on between 400~700 ℃.

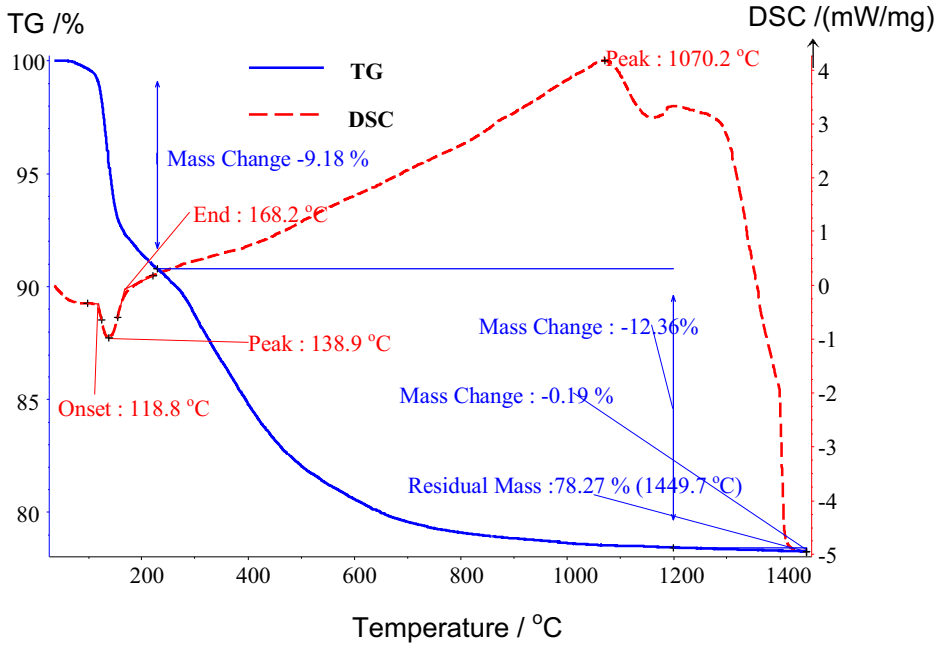

Fig. 3. DSC and TG results of the intumescent coating system

Therefore it could be suggested that the rapid decrease of mass within the system is due to loss of water from sodium silicate and Kaolinite until 200℃ and then gradual decrease thereafter is from dehydration of Kaolinite. This could be supported by the analysis of MS TG-MS measurements shown at Figure 4. This indicates that most of the evolving gas is only water and hydroxide ion. After the intumescent process the system is structured by several 10~100 um size pores constructed with wall thickness of single order um or less. This could be seen from the SEM image at fully expanded state of a cross sectional one after sample was experienced at 600 ℃ (see Figure 2)

Because of the weight decreases until ca 1200℃, thermally treated samples at every 100℃ were prepared to measure more reliable thermal properties at dynamic state. Density, heat capacity and thermal diffusivity were measured at each temperature state and presented at Figures 5~8. As could be observed by TG data after 200 ℃ gradual weight decreases due to dehydration process appears. This causes linear trend of weight and density decreases through out the measured temperature range. Comparing with the dried coating at the initial state, density decreases over 88% at 200℃ and 92% at 700℃ could be observed. The dehydration process also causes gradual decrease of heat capacity. Thermal diffusivity measurements are presented at Figure 7.

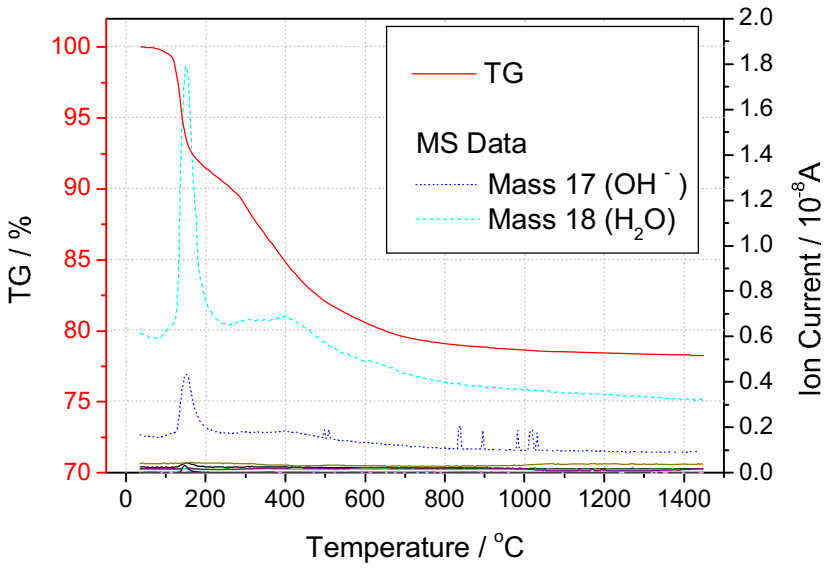

Fig. 4. TG and MS spectra results

These measurements and a mathematical equation (1) allow calculating thermal conductivity changes and the values are shown at Figure 8. As could be seen at the figure thermal conductivity slightly decreases from 200 ℃ to 400 ℃ then increases until 600 ℃, which is near the starting value at 200℃. Comparing with the increasing thermal conductivity values of general materials without phase or chemical structural changes, the investigated system holds the low value from 200℃ to 700℃and this allows the system applicable for passive fire protection

$$\lambda = \alpha \rho C_p \tag{1}$$

where λ is the thermal conductivity, α the thermal diffusivity, ρ the density and C_p the heat capacity

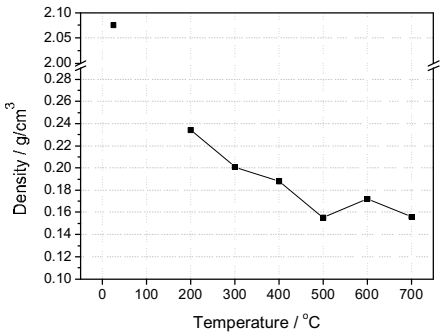

Fig. 5. Density changes as a function of temperature

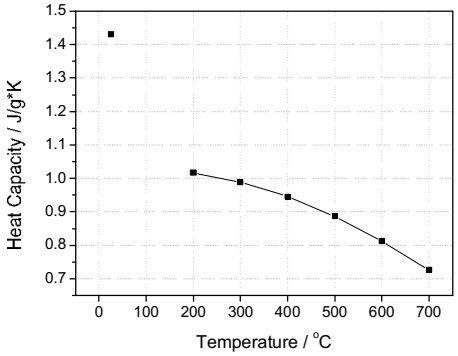

Fig. 6. Heat capacity changes as a function of temperature

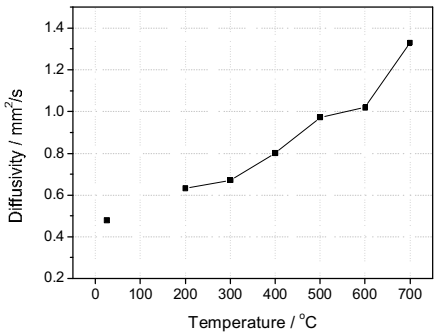

Fig. 7. Thermal diffusivity changes as a function of temperature

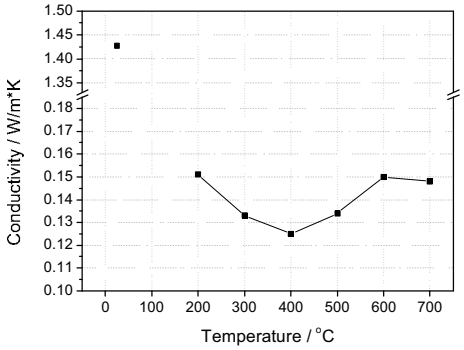

Fig. 8 Thermal conductivity changes as a function of temperature

4 SUMMARY AND ACKNOWLEDGMENT

The present study describes methods to characterise thermal properties of intumescent coating system of which thermophysical values changes as a function of temperature. For the presented intumescent coating system, lab scale experiments of measuring thermophysical properties including thermal diffusivity and specific heat constant could be enough to represent overall system.

Due to the nature of the intumescent coating system, at different temperature density, specific heat constant and thermal diffusivity changes so samples were prepared to represent at different temperature and the above thermal properties were measured. When the system was experienced at higher temperature, density and heat capacity constants decreased but thermal diffusivity increased. Hence thermal conductivity of the system could be kept similar state until 700 ℃.

The authors would like to thank Eunho Lee at Ajou University for valuable helps during LFA experiments and Hitem co. ltd for kindly supplying FC-Max samples. The work presented in this paper was undertaken as part of the research projects issued by Ministry of Knowledge Economy and Ministry of Land, Transport and Maritime Affairs. The authors gratefully acknowledge the financial assistance of the ministries.

5 REFERENCES

[1] Duquesnea, S., Delobela R., Brasa, M. and Caminob, G., Polymer *Degradation and Stability* 77 (2002) 333-344

[2] Duquesnea, S., Bras, M. L., Bourbigot, S., Delobel, R., Camino, G. C., Eling, B., Linsay, C., and Roels, T, *Polymer Degradation and Stability* 74 (2001) 493-499

[3] Zverev, V. G., Gol'din, V. D., Nesmelov, V. V., and Tsimbalyuk, A. F. *Combustion, Explosion and Shocks Waves*, Vol. 34 (1998) 198-205

[4] Koo J. H., *Fire Technology* 34 (1998) 59-71

[5] Langille, D., Nguyen, D. and Veinot, D. E., *Fire Technology* 35 (1999) 99-110

[6] www.hitem.co.kr

[7] Vauhan, F., Clay *Microporous and Meroporous Materials* 2 (1955) 265-274

[8] Selvam, T., Bandarapu, B., Mabande, G.T.P., Toufar, H., and Schwieger, W *Microporous and Meroporous Materials* 64 (2003) 41-50

STRESS-STRAIN RELATIONSHIP OF REINFORCING STEEL
Subjected to Tension and High Temperature

Marian Abramowicz [a], Robert Kowalski [b]

[a] Main School of Fire Service, Warsaw, Poland
[b] Warsaw University of Technology, Poland

INTRODUCTION

Due to popularisation of legal regulations [1] and Eurocodes [2, 3, 4] one can expect that in the nearest future during analyses of especially important buildings or buildings where people's safety is especially threatened more and more often fire is going to be considered the accidental design situation. It means that calculations of load bearing capacity of RC elements subjected to fire conditions will be required more and more often. In these calculations an appropriate estimation of stress-strain relationship of reinforcing steel plays a crucial role.

When separated structural elements are analysed the estimation of real values of reinforcement elongations is necessary for cross-section load bearing capacity calculation. When a part of a structure is considered or when a global structural analysis is performed the appropriate estimation of reinforcement elongations is also necessary for cross-sections stiffness decrease calculation. The appropriate estimation of element stiffness decrease is necessary for prediction of internal forces redistribution which often appears due to fire. Additionally in some cases as a result of stiffness decrease and significant deflections of elements heated up to high temperature a secondary static scheme of the structure might appear.

The basic stress-stain relationship of reinforcing steel subjected to high temperature is given in Eurocode [4] but before taking Eurocode model into calculations concerning fire design situation some comments and considerations should be given.

1. WAYS OF TESTING STEEL HEATED UP TO HIGH TEMPERATURE

In room temperature analyses the mechanical properties of reinforcement are usually considered in two coordinate system stress-strain (σ-ε). In analyses concerning fire design situation the third coordinate (temperature (θ)) appears. However, testing specimens in presence of three variable parameters (σ-ε-θ) could be difficult and would not lead to satisfying practical results. As a result in practice two the most important ways of testing reinforcing bars subjected to high temperature are usually used [5, 6]:

- at constant temperature (steady temperature state),
- at variable (increasing) temperature.

When the first type of testing is performed the specimens are at first heated up to high temperature. This temperature takes various values but it is kept constant in each particular test. At constant high temperature values the stress-strain relationships are examined. The way of testing is usually more or less the same as the one used at room temperature. As a result the tests performed at constant high temperatures are relatively easy to realise in practice and their results can be compared with the results obtained in room temperature tests. The Eurocode [4] model is based on the test results performed at constant temperature [5].

When the second type of testing is performed the specimens are at first loaded. The level of stress is various but it is kept constant in each particular test. During the test the specimens are heated up and the elongation (in practice displacement) is measured. In this way the temperature-strain relationships for various stress values are obtained.

Before comparing these two ways of testing it is worth to have a brief look at the problem of steel elongation at high temperature. The total elongation of reinforcing bar heated up to high temperature (ε_{tot}) can be expressed as the sum of three components as follows [5, 7]:

$$\varepsilon_{tot} = \varepsilon_0 + \varepsilon_\sigma + \varepsilon_{cr} . \tag{1}$$

In formula (1):

ε_0 – is the free thermal steel strain (appearing without any load action),

ε_σ – is the elongation appearing due to load action; sometimes the ε_σ elongation can be divided in two parts: the elastic and the ductile part but in the Authors' opinion the division of ε_σ is not important from the practical fire design analyses point of view,

ε_{cr} – is the creep elongations; it appears due to long term simultaneous action of load and high temperature.

In the tests performed at constant temperature the specimens are at first heated up and after that the measurement of the elongation begins. As a consequence the free thermal steel strain (ε_0) is usually neglected in the test results. In addition due to the relatively short time of the stress-strain relationship testing the significant part of the creep elongation (ε_{cr}) is also neglected. Reassuming it can be noticed that during the tests performed at constant high temperature only the elongation appearing due to the load action (ε_σ) is measured. The test performed at constant high temperature does not simulate the real conditions to which the structural elements are subjected during the real fire.

The real fire conditions can be simulated during the tests performed at variable (increasing) temperature. The reinforcing bars of real structural elements are stressed before the fire starts. During the fire the bars are heated up while stressed. In this conditions the total bar elongation consists of the sum of the free thermal strain (ε_0), the elongation appearing due to the load action (ε_σ) and the part of the creep elongation (ε_{cr}). The significance of this part depends on the rate of heating. When the rate of heating simulates bar temperature increase during the fire the test results can be appropriate for analyses of structural elements stiffness decrease.

2. EUROCODE [4] MODEL ANALYSIS

The basic assumption of Eurocode [4] model gives a general stress-strain relationship shown in Fig. 1. This relationship consists of three line segments and the part of ellipse inscribed between them. Mathematical formulas of the ellipse and the coefficients necessary for the calculation of values of steel mechanical properties appearing on the vertical axis are given in [4]. Table 1 shows the examples of the coefficients for hot rolled reinforcing bars.

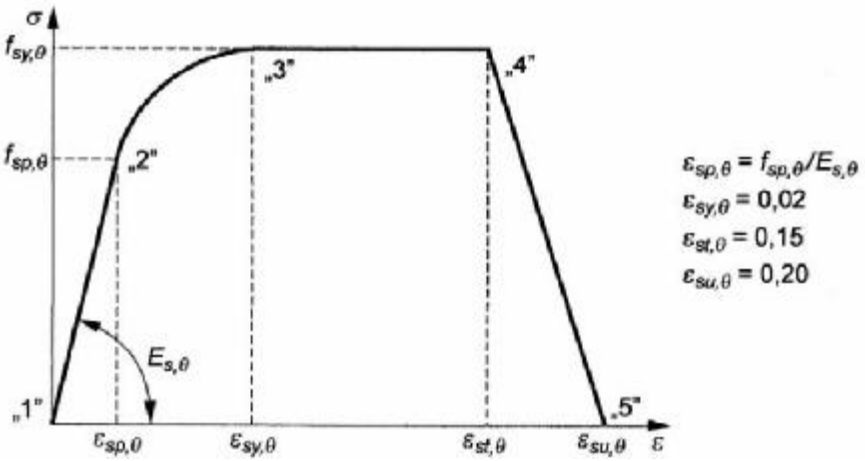

Fig. 1. The general stress-strain relationship for reinforcing steel heated up to high temperature [4]

Table 1. Coefficients for calculation of hot rolled steel mechanical properties at high temperature [4]

Temperature (θ), °C	Yield strength	Proportional limit	Modulus of elasticity
	$f_{sy,\theta}/f_{yk}$	$f_{sp,\theta}/f_{yk}$	$E_{s,\theta}/E_s$
20	1.00	1.00	1.00
100	1.00	1.00	1.00
200	1.00	0.81	0.90
300	1.00	0.61	0.80
400	1.00	0.42	0.70
500	0.78	0.36	0.60
600	0.47	0.18	0.31
700	0.23	0.07	0.13
800	0.11	0.05	0.09
900	0.06	0.04	0.07
1000	0.04	0.02	0.04
1100	0.02	0.01	0.02
1200	0.00	0.00	0.00

For practical use of Eurocode [4] model it is necessary to put the values calculated according to the Tab. 1 into the relationship shown in the Fig. 1. However, doing this one can realise that the abscissa of point „2" in the Fig. 1 is given as $\varepsilon_{sp,\theta} = f_{sp,\theta} / E_{s,\theta}$, the value of proportional limit $f_{sp,\theta}$ depends on f_{yk}, and $E_{s,\theta}$ depends on E_s = 200 GPa. As a result the value of f_{yk} has to be assumed for calculation of the elongation $\varepsilon_{sp,\theta}$. It means that it is impossible to prepare the general relationship with relative values of reinforcing steel mechanical properties on vertical axis. Figure 2 shows the examples of stress-strain relationships prepared by the Authors for hot rolled reinforcing steel of the yield strength of f_{yk} = 500 MPa.

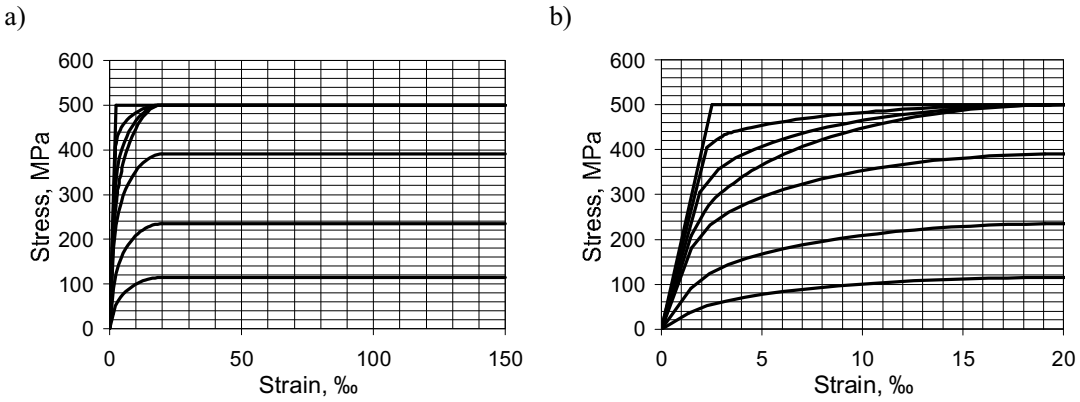

Fig. 2. Stress-strain relationships of hot rolled reinforcing steel (f_{yk} = 500 MPa) at high temperatures. Looking from the left side of the figure the successive lines refer to the temperature 100, 200, 300, 400, 500, 600 and 700 °C respectively: a) in the strain range of 0-150‰, b) the part of Fig. a in the strain range of 0-20‰.

Comparing figures 1 and 2a one can notice that the relationship shown in the Fig. 1 does not respect the scale of the horizontal axis. Almost all area of Fig. 2a is covered by the horizontal lines situated between strain values of 20 and 150‰. These lines can influence the calculation results only when advanced analysis is performed. When simplified calculation method is used the appearance of reinforcement elongation in point „3" in the Fig. 1 means that the cross-section ultimate limit state is reached. As a result in practical simplified analysis the cross-section ultimate limit state will always be reached when the steel elongation is equal to 20‰ irrespectively of the temperature.

In the Authors' opinion the point „3" should rather take a variable placement on the horizontal axis of Fig. 1. The elongation $\varepsilon_{sy,\theta}$ could be lower than 20‰ for the relatively low temperature and

higher than 20‰ for the relatively high temperature. It should also be reminded that in the original version [5] of the Eurocode [4] model the line segment situated between points „3" and „4" in the Fig. 1 was not horizontal but took higher and higher values with the strain increase.

The Eurocode [4] model is based on the test results performed in steady temperature state conditions [5]. It means that the steel elongation obtained according to the Fig. 1 is only this part of the total reinforcing bar elongation which appears due to stress (ε_σ). The Authors suggest that for RC elements calculation in fire the free thermal steel elongation (ε_0) should be added to elongation calculated according to the Fig. 1. The Fig. 3 shows the stress-strain relationships for reinforcing steel (f_{yk} = 500 MPa) prepared by the Authors. The elongation shown in the Fig. 3 is the sum of the values taken from the Fig. 2b and free thermal steel elongation estimated according to Eurocode [4] recommendation. Comparing figures 2b and 3 one can conclude that the elongation of RC elements bars can be larger than the one calculated according to the Eurocode [4] model.

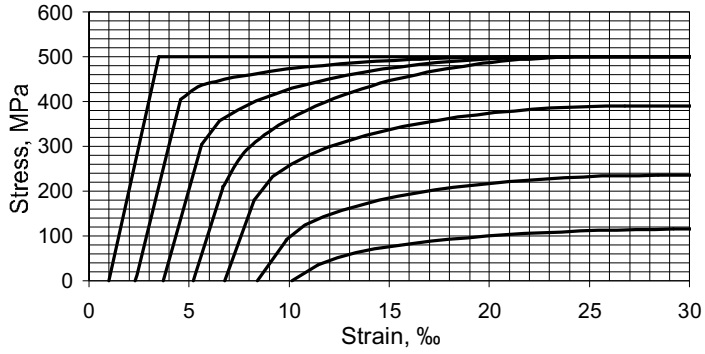

Fig. 3. Stress-strain relationships of hot rolled reinforcing steel (f_{yk} = 500 MPa) at high temperatures. Looking from the left side of the Figure the successive lines refer to the temperature 100, 200, 300, 400, 500, 600 and 700 ^{o}C respectively. The strain is the sum of values taken form Fig. 2b and free thermal steel elongation estimated according to [4] recommendation.

3. REINFORCEMENT ELONGATION IN HEATED UP RC BEAMS

The sum of the average strain values of the external cross-section fibres can be estimated on the base of the beam deflection. For that purpose, one should consider generally known formulas. The beam deflection is expressed with the following formula:

$$a = \alpha \cdot \frac{Ml^2}{EJ}. \tag{2}$$

The beam axis curvature can be expressed with two formulas:

$$\frac{1}{r} = \frac{M}{EJ} \tag{3}$$

and

$$\frac{1}{r} = \frac{\varepsilon_s + \varepsilon_c}{d}. \tag{4}$$

In the formula (4) ε_s is the average value of reinforcing bar elongation, ε_c is the average value of the contraction of the external fibre of concrete compressed zone and d is the cross-section depth.

With the above formulas (2, 3 and 4) the sum of the average values of concrete and reinforcement strains can be expressed as follows:

$$\varepsilon_s + \varepsilon_c = \frac{d \cdot a}{\alpha \cdot l^2}. \tag{5}$$

When the ratio of ε_s to the sum of $\varepsilon_s + \varepsilon_c$ is assumed the average values of ε_s can be estimated according to the formula (5) on the base of the beam deflection.

The Authors tested RC beams under simultaneous action of high temperature and constant load. The cross-section of tested beams was b x h = 12 x 14 cm and their length was 120 cm. Two types of concrete: C30/37 and C60/75, with siliceous aggregate and three different reinforcement ratios were used. The main reinforcement of each beam consisted of two bars. Cold rolled 6 mm diameter bars of f_y = 674 MPa steel and hot rolled 10 and 14 mm diameter bars of f_y = 580 MPa steel were used. The concrete cover of the bars in each beam was 15 mm.

The beams were put into the furnace chamber, heated up to the temperature of 670 °C and immediately loaded to the load level of 54 % of their load bearing capacity obtained experimentally at room temperature. The temperature inside the chamber increased to the value of 800 °C in about 15 minutes and then it was kept constant. The beams were tested under simultaneous action of high temperature and constant load up to the failure. During the test the deflection of beams and the temperature inside some places of their cross-sections were measured. More details about specimens and testing procedure can be found in [8, 9].

Table 2 shows the average beam deflections and the values of the average reinforcement bar elongation estimated on the base of beam deflection according to formula (5) and assumption shown in the column 2 of the Table 2 at various temperatures. Because the deflections of beams made of C30/37 and C60/75 concrete were more or less equal in the Table 2 only the average values of both concrete type beams are shown.

Table 2. Average values of beam deflection and estimated average reinforcement elongations at various temperatures

Reinforcement type	$\frac{\varepsilon_s}{\varepsilon_s + \varepsilon_c}$	Average beam deflection, mm Average reinforcement elongation (ε_s), ‰				
		100°C	200°C	300°C	400°C	500°C
1	2	3	4	5	6	7
2 ø 6	0.95	3.6 3.49	6.1 5.91	8.6 8.34	12.5 12.07	23.1* 22.34*
2 ø 10	0.89	5.8 5.22	7.8 7.08	11.2 10.12	15.9 14.44	33.6 30.46
2 ø 14	0.77	8.0 6.28	11.1 8.68	14.8 11.63	20.4 15.99	41.4 32.25

* The deflection and the elongation obtained at the temperature of 475°C.

Figure 4 shows the comparison of the average reinforcement elongations obtained in tested beams (Tab. 2) and the elongations calculated by the Authors according to the Eurocode model [4].

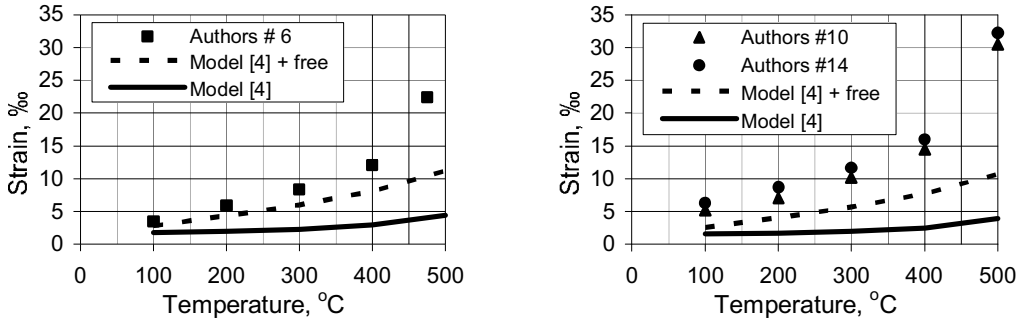

Fig. 4. Comparison of reinforcement elongation obtained in tested beams and Eurocode [4] prediction: marks – the Authors' test results, solid line – elongation calculated according to the Eurocode [4] stress-strain relationship model, detached line – the sum of Eurocode [4] model and free thermal steel strain

In the Fig. 4 the marks referring to reinforcement elongations obtained in tested beams are situated much higher than both lines calculated according to the Eurocode [4] model. It might suggest that the elongation of real bent RC elements is higher than values estimated according to Eurocode [4] due to the steel creep elongation (ε_{cr}) or that Eurocode [4] model underestimates reinforcement elongation.

4. CONCLUSIONS

The stress-strain relationship recommended in the Eurocode [4] is based on the test results performed in steady temperature state conditions. This type of testing does not simulate the conditions to which the real RC structural elements are subjected during the real fire.

The reinforcing bars of real RC structural elements are stressed before the fire starts and during the fire the bars are heated up while stressed. The real fire conditions can be simulated by the tests performed under constant load and increasing temperature. In these tests the sum of the free thermal steel strain and the elongation appearing due to load action is measured.

When the stiffness decrease of bent RC structural elements in fire is going to be considered the reinforcement elongation should be calculated according to the Eurocode [4] as the sum of the elongation estimated on the base of stress-strain relationship and free thermal steel elongation.

REFERENCES

[1] Interpretative Document (to Council Directive 89/106/EEC), Essential Requirement No 2 "Safety in Case of Fire".

[2] EN 1990: 2002: Eurocode: Basis of structural design.

[3] EN 1991-1-2:2002: Eurocode 1: Actions on structures – Part 1-2: General actions – Actions on structures exposed to fire.

[4] EN 1992-1-2: 2004: Eurocode 2: Design of concrete structures – Part 1.2: General rules - Structural fire design.

[5] Anderberg Y.: Modelling Steel Behaviour. Fire Safety Journal 13, 1988, p. 17-26.

[6] Kirby B.R., Preston R.R.: High Temperature Properties of Hot-rolled, Structural Steels for Use in Fire Engineering Design Studies. Fire Safety Journal 13, 1988, p. 27-37.

[7] Skowroński W.: Fire Safety of Metal Structures. PWN, Warsaw 2004.

[8] Kowalski R.: Load bearing capacity calculation of bent RC elements in fire (in Polish). Publishing House of the Warsaw University of Technology. Scientific Works. Building Engineering 149/2008.

[9] Kowalski R.: Deformation and Load Bearing Capacity of RC Flexural Cross-Section Subjected to Fire. 7th International Congress Concrete: Construction's Sustainable Options. Dundee, Scotland, 2008. Conf. Proc. Concrete for Fire Engineering p. 35-46.

Application of Structural Fire Design, 19-20 February 2009, Prague, Czech Republic

DECOMPOSITION OF INTUMESCENT COATINGS: COMPARISON BETWEEN NUMERICAL METHOD AND EXPERIMENTAL RESULTS

Luís M.R. Mesquita[a], Paulo A.G. Piloto[a], Mário A.P. Vaz[b] and Tiago M.G. Pinto[a]
[a] Polytechnic Institute of Bragança, Applied Mechanics Department, Portugal.
[b] University of Porto, Faculty of Engineering, Portugal.

INTRODUCTION

Passive fire protection materials insulate steel structures from the effects of the elevated temperatures that may be generated during fire. They can be divided into two types, non-reactive, of which the most common types are boards and sprays, and reactive, being intumescent coatings an example. They are available as solvent or water based systems applied up to approximately 3[mm]. One problem associated with the use of such systems is the adhesion of the charred structure to the steel element during fire and upon it. It is very important that the char remains in the steel surface to insure the fire protection.
The intumescent chemistry has changed little over the past years and almost all coatings are largely based on the presence of similar key components. The chemical compounds of intumescent systems are classified in four categories: a carbonisation agent, a carbon rich polyhydric compound that influences the amount of char formed and the rate of char formation; an acid source, a foaming agent, which during their degradation release non-flammable gases such CO2 and NH3, [1].
Activated by fire or heat, a sequential chemical reaction between several chemical products takes place. At higher temperatures, between 200-300 [ºC], the acid reacts with the carboniferous agent. The formed gases will expand, beginning the intumescence in the form of a carbonaceous char.
Different models handle the intumescent behaviour with char forming polymers as a heat and mass transfer problem. Other existing models provide a suitable description regarding the intumescence and char formation using kinetic studies of thermal degradation, accounting the complex sequence of chemical reactions, thermal and transport phenomenon, [[2]-[5]].
Due to the thermal decomposition complexity of intumescent coating systems, the models presented so far are based on several assumptions, being the most relevant the consideration of one-dimensional heat transfer through material, temperature and space independent thermal properties and the assumption of a constant incident heat flux where the heat losses by radiation and convection are ignored, [3]. Some authors also assume that the thermochemical processes of intumescence occur without energy release or energy absorption, [6]. Results show that the insulation efficiency of the char depends on the cell structure and the low thermal conductivity of intumescent chars result from the pockets of trapped gas within the porous char which act as a blowing agent to the solid material.
The authors, in a previous work, considering the results obtained from coated steel plates tested in a cone calorimeter studied the intumescence as one homogenous layer. The steel temperature variation was considered and with the intumescence thickness time variation an inverse one-dimensional heat conduction problem (IHCP) was applied to determine the intumescence effective thermal conductivity and thermal resistance [7].
This work presents an experimental study to assess the performance of water-based intumescent paints used as a passive fire protection material. These tests were performed in a cone calorimeter, in steel plates coated with two different paints, three dry film thicknesses and considering two different radiant heat fluxes. During tests, among other quantities, the steel temperature, the intumescence mass loss and thickness variation were measured. A numerical model is also presented to study the intumescence behaviour. The paint thermal decomposition numerical model is based on the conservation equation of energy, mass and momentum.

1. EXPERIMENTAL TESTS PERFORMED IN THE CONE CALORIMETER

To assess the performance of two commercial water-based intumescent paints a set of experimental

tests was performed in a cone calorimeter, see Fig. 1 and Fig. 2. The steel plates are 100 [mm] squared and 4, 6 [mm] thick, coated in one side with different dry film thicknesses and tested in a cone calorimeter as prescribed by the standard ISO5660, [8]. Temperatures are measured by means of four thermocouples, type k, welded at the plate in the heating side and at the opposite side, at two different positions. The samples were weighted before and after of being coated allowing for the initial coating mass. The dry thickness was also measured in 16 different points, being the mean values and the standard deviation presented in the Fig. 1.

Specimens identification					Initial mass [g]	Final mass [g]	Coating mass [g]	Thick (mean) [µm]	σ (SD) [µm]
B	35	4	0.5	1	366,73	375,36	8,63	571	41,6
B	35	4	0.5	2	365,38	374,88	9,5	626	38,6
B	35	4	0.5	3	364,95	373,95	9	603	49,5
B	35	4	1.5	1	365,63	390,10	24,47	1510	70,2
B	35	4	1.5	2	365,82	391,42	25,6	1570	64,1
B	35	4	1.5	3	364,80	390,67	25,87	1580	66,5
B	35	4	2.5	1	365,49	409,85	44,36	2640	90,9
B	35	4	2.5	2	366,29	409,12	42,83	2560	89,0
B	35	4	2.5	3	366,40	407,77	41,37	2510	85,7
B	75	4	0.5	1	362,92	371,94	9,02	581	35,9
B	75	4	0.5	2	366,00	375,97	9,97	662	53,9
B	75	4	0.5	3	367,53	377,53	10	631	31,2
B	75	4	1.5	1	366,27	390,71	24,44	1530	79,5
B	75	4	1.5	2	364,69	389,63	24,94	1550	67,8
B	75	4	1.5	3	359,09	384,05	24,96	1560	74,9
B	75	4	2.5	1	359,79	399,66	39,87	2520	211
B	75	4	2.5	2	364,28	405,30	41,02	2520	91,4
B	75	4	2.5	3	364,80	404,97	40,17	2490	126
B	35	6	0.5	1	528,60	537,10	8,5	533	56,7
B	35	6	2.5	1	528,91	571,74	42,83	2570	105
B	75	6	0.5	1	525,47	534,86	9,39	607	65,9
B	75	6	2.5	1	529,04	570,00	40,96	2610	75,8

Specimens identification					Initial mass [g]	Final mass [g]	Coating mass [g]	Thick (mean) [µm]	σ (SD) [µm]
A	35	4	0.5	1	363,77	373,56	9,79	575	47,3
A	35	4	0.5	2	363,82	373,35	9,53	574	56,4
A	35	4	0.5	3	364,54	373,19	8,65	528	60,4
A	35	4	1.5	1	361,10	387,74	26,64	1670	107
A	35	4	1.5	2	362,17	388,06	25,89	1610	72,2
A	35	4	1.5	3	361,38	385,42	24,04	1450	84,9
A	35	4	2.5	1	362,81	403,37	40,56	2530	149
A	35	4	2.5	2	365,81	407,89	42,08	2590	122
A	35	4	2.5	3	363,49	415,12	51,63	2590	121
A	75	4	0.5	1	363,46	372,34	8,88	549	60,3
A	75	4	0.5	2	363,58	373,20	9,62	581	61,1
A	75	4	0.5	3	368,44	377,85	9,41	582	48,6
A	75	4	1.5	1	369,59	394,82	25,23	1510	83,7
A	75	4	1.5	2	371,11	396,24	25,13	1530	87,7
A	75	4	1.5	3	364,87	391,13	26,26	1620	98,7
A	75	4	2.5	1	366,97	407,71	40,74	2590	122
A	75	4	2.5	2	365,11	404,90	39,79	2590	134
A	75	4	2.5	3	370,60	410,77	40,17	2530	167
A	35	6	0.5	1	527,37	535,05	7,68	476	33,1
A	35	6	2.5	1	526,65	565,71	39,06	2420	150
A	75	6	0.5	1	522,90	530,58	7,68	494	33,9
A	75	6	2.5	1	525,71	564,89	39,18	2490	112

Fig. 1. Set of experimental tests. Reference: Paint/Heat Flux/Steel Thick./Dry Thick/Test Nº.

Fig. 2. Coated steel plates, with fixed thermocouples. Tested samples at 35 [kW/m2] and at 75 [kW/m2]. Reference and position of the thermocouples.

Between the steel plate and the sample older two silicate plates were used to put the specimen in place and also a thermocouple was placed to measure its temperature variation. The distance between the sample surface and the heater remained unchanged, at approximately 60 [mm], which means that with the increasing intumescence the top of the sample came closer to cone surface. Due to the large amount of results, only a set of samples will be referenced in this paper.

1.1 Experimental Results

The temperature evolution in a steel plate without protection was also tested to attain the efficiency of this fire protection. The measured temperatures are presented in the Fig. 3 for a radiant heat flux of 35 [KW/m^2] and then resetting the cone to 75 [KW/m^2].

Fig. 4 represents the mass loss of each sample and shows a variation almost linear with time mainly for a heat flux of 35 [kWm^{-2}].

Using discrete frames obtained from digital camera during tests and by image processing techniques using Matlab, the intumescence development was measure over time. Fig. 5 presents the intumescent development (free boundary L(t)) for specimens with paint A and B, different thicknesses and radiant heat fluxes.

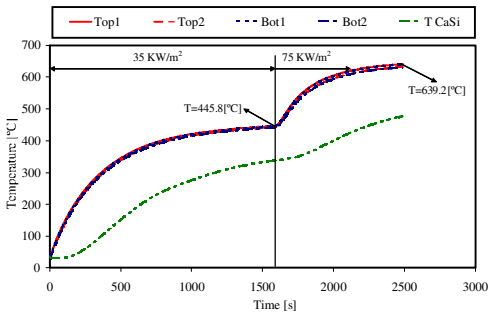

Fig. 3. Measured temperature in the steel plate without protection.

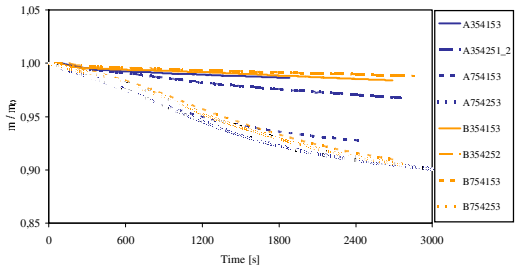

Fig. 4. Measured mass loss with time.

Higher intumescence may be noticed in sample right region coincident to the thermocouples wire position responsible for coating accumulation. The presented values are mean values determined from four central measures.

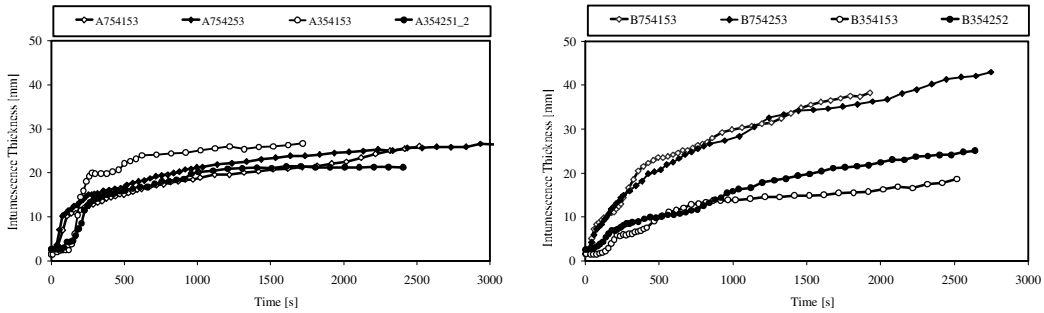

Fig. 5. Intumescence thickness mean values of four central measurements.

The figures shown that for the lower heat flux the intumescence becomes stable, but for the higher it continues to increase. Coating A presents a higher expansion at the initial stage compared to the coating B. For longer exposure periods of exposure coating B continues to expand.

The steel temperature profiles and temperatures at the middle of the silicate plates are reported in Fig. 6 and Fig. 7. Measured values from the thermocouples welded on the bottom of the plate are very close to the temperatures at the top. For the same heat flux, the time to reach a same temperature increases with the increase of the dry thickness.

The behaviour is very similar for both coatings, but for all cases the time to reach, for example a temperature of 200 [°c] is always higher when the paint B is used. For these conditions it gives an improved fire protection.

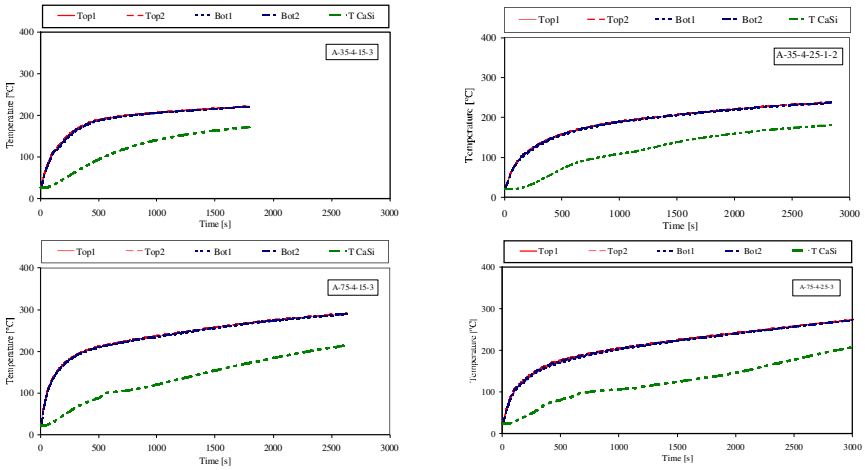

Fig. 6. Temperature variation of steel and silicate plates for coating A.

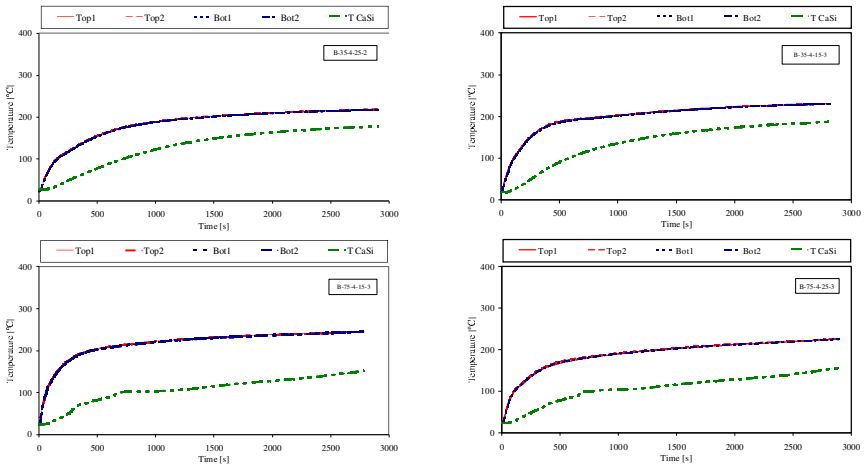

Fig. 7. Temperature variation of steel and silicate plates for coating B.

2 MATHEMATICAL MODEL OF THE INTUMESCENCE BEHAVIOUR

The problem to determine the temperature field in an intumescent material involves the solution of a phase transformation problem with two ore more moving boundaries that characterize its state, initial, softened and carbonaceous char. Different methodologies can be found in the literature to model the thermal decomposition of a polymer or polymer based materials. The methodology followed in this work was to consider that the decomposition occurs not only at the outside surface but also inside, for temperatures above the pyrolysis temperature, T_p. In this case the moving boundary regression rate must be determined considering the motion of all domain. This strategy implies that a mass diffusion term needs to appear in the energy equation due its motion. This term was disregarded due to the small thickness of the virgin layer for this types of applications, about 1-3 [mm].

Considering a first order reaction, the mass loss is given by

$$\dot{m}(T(x,t)) = \frac{\partial \rho_v}{\partial t} = -\rho_v A_0 \, e^{-\frac{E_0}{RT(x,t)}} \qquad for \quad T \geq T_p \tag{1}$$

where $\dot{m}$ is the local mass loss [kg. $m^{-3}s^{-1}$] , T (x,t) is the temperature at point x at instant t , A_0 is the pre exponential factor [s^{-1}], E_0 the activation energy [$J.mol^{-1}$], and R the universal gas constant [$J.mol^{-1}.K^{-1}$]. The position of the moving boundary is obtained by summing all the mass loss and dividing by the specific mass.

The energy equation for the steel and virgin layers is based on the one-dimensional conduction heat equation.

The conservation equation for the solid virgin material phase is given by

$$\frac{\partial \rho_v V_v}{\partial t} = -\dot{w}_v^{'''d} V_v \tag{2}$$

Where $\dot{w}_v^{'''d}$ represents the destruction rate of virgin material per unit volume, originated by the thermal decomposition. The virgin material decomposition produces a fraction of gas, equal to the porosity, φ, and a solid char fraction equal to $(1-\varphi)$.

The formation rate of char and gas mass is:

$$\dot{w}_{gas}^{p} = -\left(1-\frac{\rho_c}{\rho_g}\right)\chi\rho_v A\frac{ds(t)}{dt} \qquad \dot{w}_{char}^{p} = -\left[1-\left(1-\frac{\rho_c}{\rho_g}\right)\chi\right]\rho_v A\frac{ds(t)}{dt} \tag{3}$$

χ represents the fraction of the bulk density difference between the virgin and char materials that is converted to gas. In this study the value used was $\chi = 0.66$, [9].

The conservation of gas mass equation is given by eq. (4).

$$\frac{\partial(\rho_g \varphi)}{\partial t} + \frac{\rho_g \varphi}{V}\frac{\partial V}{\partial t} + \frac{\partial \dot{m}_g^{"}}{\partial x} = 0 \tag{4}$$

In the previous equation $\partial V/\partial t$ represents the intumescence rate. The gas mass flux, $\dot{m}_g^{"}$, is calculated accordingly to Darcy's law and it is assumed that the gases present in the intumescent material behave as a perfect gas. The thermodynamic properties are related by the ideal gas law and, assuming that the gas is a mixture of $50wt\%CO_2$ and $50wt\%H_2O$, the generated gas molar mass used in the model M_g is $31[g/mol]$.

The conservation of gas mass equation with the Darcy's and the ideal gas laws combined can be used to give a differential equation for the pressure inside the intumescence. In the numeric calculations, the intumescence rate is assumed to be known, provided by the experimental results, so the pressure calculation is disregarded being assumed that the internal pressure is constant and equal to the atmospheric pressure. An energy equation for the conservation of energy within the intumescence zone can be obtained by combining the energy equation for the gases with that of the solid char material. The equation for the conservation of energy per unit bulk volume can be written as:

$$(\rho Cp)_{eff}\frac{\partial T}{\partial t} + \frac{\partial}{\partial x}\left(\dot{m}_g^{"} T_g Cp_g\right) = \frac{\partial}{\partial x}\left(k_{eff}\frac{\partial T}{\partial x}\right) - CpT\frac{\partial \rho}{\partial t} - (\rho Cp)_{eff}\frac{T}{V}\frac{\partial V}{\partial t} \tag{5}$$

where $(\rho Cp)_{eff} = \varphi\rho_g Cp_g + (1-\varphi)\rho_c Cp_c$ and $k_{eff} = \varphi k_g + (1-\varphi)k_c$.

The effective thermal conductivity for the intumescence bulk material, including gas and char, is equal to the thermal conductivity of the gas per unit bulk volume, plus that of the solid material. The same thing applies to the effective heat capacity.

In the steel plate back surface it is assumed an adiabatic boundary condition and at the boundary steel/virgin layers it is assumed a perfect thermal contact. At the moving front, the boundary conditions are:

$$\begin{aligned} k_v\frac{\partial T}{\partial x} &= \varepsilon\dot{q}_r^{"} - \varepsilon\sigma\left(T^4 - T_a^4\right) - h_c\left(T - T_a\right) \qquad for \qquad T(s(t),t) < T_P \\ k_v\frac{\partial T}{\partial x} - k_c\frac{\partial T}{\partial x} &= Q_H \qquad for \qquad T(s(t),t) = T_P \end{aligned} \tag{6}$$

In which Q_H is the heat flux due to the endothermic decomposition of the virgin material, given by $Q_H = -h_p\rho_v\dot{s}(t)$, where h_p represents the decomposition enthalpy. A wide range of values are reported in the literature for the heat of pyrolysis and go from a few units to units of millions. The value used in the calculations was 50 [J/kg].

The intumescent coating specific mass was measured by the pycnometer method given a value of 1360 and 1250 [kg/m^3] for the virgin coating and a value of 692.4 and 450 [kg/m^3] for the char material, for paints A and B, respectively. Steel properties are assumed constant, with a specific heat value of 600 [J/kgK] and a specific mass equal to 7850 [kg/m^3]. The intumescent coating specific heat was considered constant and equal to 1000 [J/kgK].

The mathematical model is based on the following major simplifying assumptions: there is no heat between gas and char, the thermophysical properties and the pressure at both layers are constant.

The solution method was implemented in a Matlab routine using the Method Of Lines (MOL), [10], and the integrator *ode15s* to solve the set of ordinary differential equations.

The temperature field is determined by the steel and virgin energy equations. When the front reaches the pyrolysis temperature, equal to 250 [ºc], starts to decompose and to move. Then the moving front rate is determined and the intumescence forms. The position the free boundary is set equal to the experimental results and the intumescence temperature field is determined. In each time step the virgin and char layers are remeshed.

The input parameters are listed as follows: $k_v = 0.5Wm^{-1}K^{-1}$; $k_c = 0.1Wm^{-1}K^{-1}$; $Cp_v = 2600Jkg^{-1}K^{-1}$; $Cp_c = 3000Jkg^{-1}K^{-1}$; $h_c = 20Wm^2K^{-1}$; $\varepsilon = 0.92$; $T_P = 525K$; $A_0 = 4.67e^{12}s^{-1}$.

Two case studies are presented in Fig. 8 and Fig. 9. In the first one the steel temperature variation and the moving front position are determined based on a value of the activation energy equal to $E_0 = 125 KJmol^{-1}$. The numerical results follow reasonably well the experimental values. The major differences occur at intermediate times probably because a transition state of molten polymer was not considered.

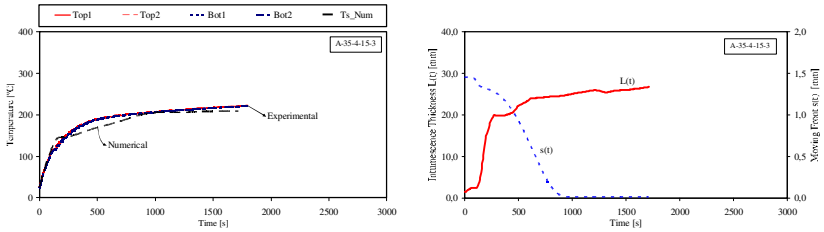

Fig. 8. Comparison of measured and computed steel temperatures and position of the moving front, $E_0 = 125 KJmol^{-1}$.

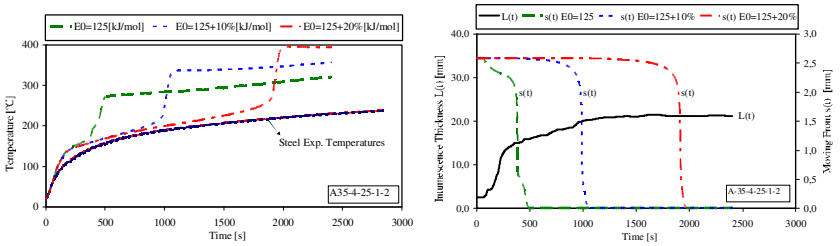

Fig. 9. Influence of the activation energy in the steel temperature and in the moving front.

Both the determined steel temperatures and the moving front are strongly dependent on the activation energy that defines the amount of mass loss of virgin paint, as presented in Fig. 9. It must be said that the value used in the simulations was obtained from the literature, but the correct value of both paints are needed. The reaction kinetics parameters can be obtained from thermogravimetric analysis.

ACKNOWLEDGMENTS

The authors acknowledge the financial support from the Portuguese Science and technology Foundation, project PTDC/EME-PME/64913/2006, "Assessment of Intumescent Paint Behaviour for Passive Protection of Structural Elements Submitted to Fire Conditions", and fellowship SFRH/BD/28909/2006. The authors acknowledge also the contribution from the paints producers: CIN, Nullifire.

REFERENCES

[1]. Duquesne, S.; Bourbigot, S. Delobel, R., "Mechanism of fire protection in intumescent coatings", European Coatings Conference: Fire Retardant Coatings II, Berlin, 2007.
[2]. Staggs J. E. J., "A discussion of modelling idealised ablative materials with particular reference to fire testing", Fire Safety Journal, Vol. 28, ,47-66, 1997.
[3]. Moghtaderi B., Novozhilov V., Fletcher, D., Kent J. H., "An integral model for the transient pyrolysis of solid materials" Fire and Materials, Vol. 21, 7-16, 1997.
[4]. Lyon R. E., "Pyrolysis kinetics of char forming polymers", Polymer Degradation and Stability, Nº 61, pp. 201-210, 1998.
[5]. Jia F., Galea E. R., Patel M. K., "Numerical Simulation of the Mass Loss Process in Pyrolizing Char Materials", Fire And Materials, Nº 23, 71-78, 1999.
[6]. Kuznetsov, G. V., Rudzinskii, V. P., "Heat transfer in intumescent heat- and fire-insulating coatings", Journal of Applied Mechanics and Technical Physics, Vol. 40, No. 3, 1999.
[7]. Mesquita, L.M.R.; Piloto, P.A.G.; Vaz, M.A.P.; Pinto, T.; "Numerical Estimation For Intumescent Thermal Protection Using One-Dimensional IHCP", WCCM8-ECCOMAS2008, ISBN: 978-84-96736-55-9, Venice, Italy, June 30 – July 5, 2008.
[8]. ISO 5660-1:2002, Reaction-to-fire tests - Heat release, smoke production and mass loss rate. Part 1: Heat release rate (cone calorimeter method), International Organization for Standardization, 2002.
[9]. C. Lautenberger, A Generalized Pyrolysis Model for Combustible Solids, Ph.D . thesis, University of California at Berkeley, Berkeley, CA, 2007.
[10]. Wouwer A.V, Saucez P., and W. E. Schiesser, "Simulation of Distributed Parameter Systems Using a Matlab-Based Method of Lines Toolbox: Chemical Engineering Applications", Ind. Eng. Chem. Res. 2004, 43, 3469-3477.

THERMAL BEHAVIOUR OF ALKALI ACTIVATED SLAG COMPOSITES
Effect of Aggregates

Pavel Rovnaník [a], Patrik Bayer [a], Pavla Rovnaníková [a]

[a] Brno University of Technology, Faculty of Civil Engineering, Brno, Czech Republic

INTRODUCTION

Portland cement is widely used as a part of many building materials among which the most common is concrete. This material is highly inflammable and does not support combustion of other material. However, its undesirable fast degradation, when exposed to very high temperature, connected with compressive strength decrease, cracking and spalling limits the utilization of concrete in constructions endangered by fire [1-3]. Concretes based on alkali activated slag (AAS) exhibit a very good resistance against high temperatures and fire [4-6]. Due to its different porosity no spalling occurs even during thermal shock treatment. This property can be improved by application of artificial thermally stabilized aggregates with low extensibility. We have examined the influence of burnt clay (chamotte) and andalusite on the behavior of alkali activated slag composite during heat loading up to 1200 °C and the mechanical properties after high temperature exposure. This study is partially focused on the interstitial transition zone between the aggregate and AAS binder.

1 EXPERIMENT

1.1 Materials

For the investigation of material properties, specimens of finely granulated blast furnace (BF) slag from Kotouč, s r.o. Štramberk activated with dried sodium silicate Portil A (Henkel AG) were prepared. Chamotte, andalusite and quartz sand were used as an aggregate. The specific surface of the slag was 380 m^2/kg and its basicity modulus was 1.07. The chemical composition of slag is given in table 1.

Table 1. Chemical composition of blast furnace slag

Component	SiO_2	Al_2O_3	Fe_2O_3	CaO	MgO	MnO	S_{total}
Content, %	37.8	6.9	0.2	34.9	12.8	0.5	0.5

Dried sodium silicate Portil A with M_s = 1.9 was used as an activator. The grain size of chamotte and andalusite aggregate was in the range 0-5 mm. The maximum grain size of standard quartz sand was 2.5 mm.

Testing Methods

The mixture of slag, activator, aggregate and water was placed into moulds of 40×40×160 mm dimension. The hardened specimens were stored in water for 28 days. Afterwards the composite was pulled out and left at an ambient temperature for 3 days. Then, the specimens were exposed to elevated temperatures 200, 400, 600, 800, 1000, and 1200 °C with 1 h dwell, and afterwards they were let cool down spontaneously. Reference samples were stored at 20 °C. The microstructure of composites was investigated by means of mercury intrusion porosimetry (Micromeritics Poresizer 9300) and electron scanning microscopy (JEOL U 3). Composition of the mixtures is listed in table 2.

Table 2. Composition of alkali activated slag and Portland cement mortars

Component	Slag	Aggregate	Portil A	Water
Content, kg/m^3	586	1758	117	235

2 RESULTS AND DISCUSSION

The properties and microstructure of AAS composites with inspected aggregates were compared with composite containing only standard quartz sand as aggregate. As reference samples we considered the specimens which were treated only at an ambient temperature. Bulk density of described specimens is presented in table 3. The compressive strengths of AAS with chamotte reached the value for AAS matrix itself [7], therefore the aggregate seems not to be a limiting factor for the mechanical properties of such composite. On the contrary, the quartz sand causes a strength decrease by approx. 20 MPa and andalusite even by 40 MPa (Fig. 1). This might be explained by weaker contacts between AAS matrix and aggregate that is, in the case of andalusite, indicated by cracks on the surface of specimens (Fig. 2). After exposure to elevated temperature, the compressive strengths gradually decrease. The trend, however, appears to be the same for all three composites, therefore it can be attributed to dehydration and decomposition of AAS matrix. Strength decrease of AAS composite with quartz above 600 °C is partly caused by phase transformation of quartz at 573 °C (α-qaurtz↔β-quartz), accompanied by the change of volume. Exposure of AAS material to temperatures above 800 °C enables the crystallization and formation of several crystalline phases, among which akermanite is predominant [5]. These phases are responsible for increase of strengths that reach 53% of original strength for AAS with chamotte, 23% for AAS with andalusite, and 36% of that obtained for AAS with quartz, respectively.

Table 3. Bulk density of alkali activated slag composites

Aggregate type	Chamotte	Andalusite	Quartz
Bulk density, kg/m^3	2230	2520	2150

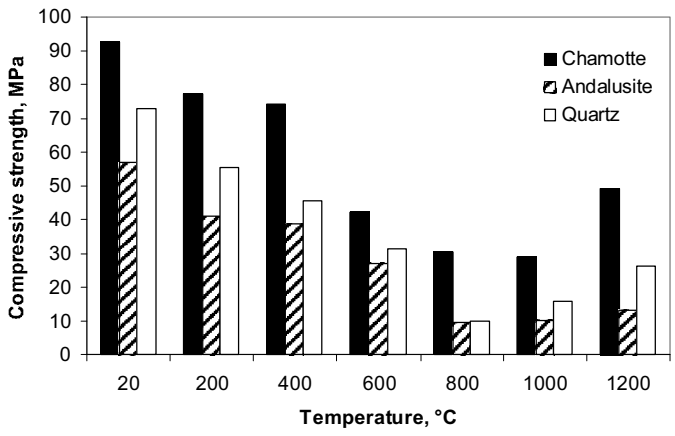

Fig. 1. Compressive strengths of AAS composites for different temperatures of exposure

Fig. 2. Cracks on the surface of andalusite composite

Flexural strengths of all AAS composites follow the same trend that has been observed for compressive strengths (Fig. 3). However, at elevated temperature the composite with chamotte performs much better values by approx. 3 MPa in comparison with AAS filled with quartz sand. Flexural strengths of heated AAS filled with andalusite are by 4 MPa lower than those obtained for

AAS with chamotte. The significant increase of flexural strength for chamotte composite after exposure to 1200 °C, that even exceeds the reference value, can be ascribed to the reaction of AAS matrix with surface of aggregates that results in the formation of tight ceramic bond.

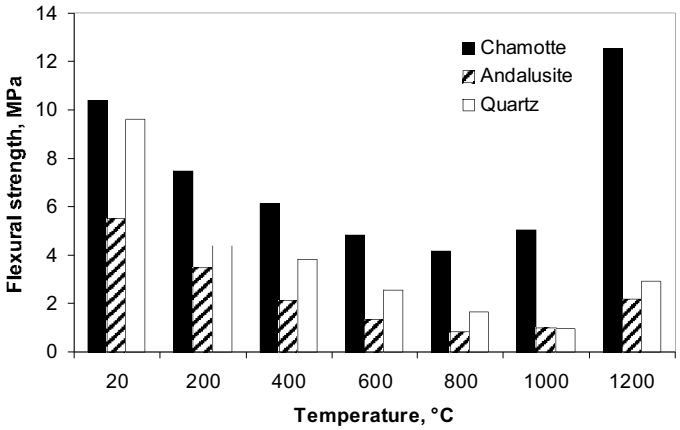

Fig. 3. Flexural strengths of AAS composites for different temperatures of exposure

The mechanical properties of inspected AAS composites after exposure to elevated temperature can be explained by changes in microstructure. Distribution of pores smaller than 100 μm for unexposed composites is almost independent of the aggregate type used, although some minor cracks were observed on specimens with andalusite. Dehydration and decomposition of AAS matrix starts upon heating that results in its shrinkage and finally in an increase of porosity. The first difference is obtained after heating to 600 °C. The porosity of quartz composite increases due to rapid reversible change between α-quartz and β-quartz modifications at 573 °C (Fig. 4).

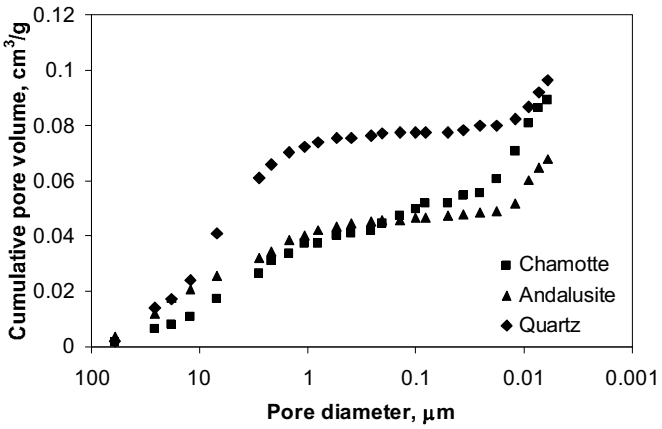

Fig. 4. Comparison of pore distribution of AAS composites after exposure to 600 °C

Upon further heating very small gel pores completely disappear and above 1000 °C only pores larger than 1 μm remain. However, the total porosity differs according to the aggregate type used (Fig. 5). The biggest apparent porosity was observed for AAS composite with quartz sand and the least porous seems to be andalusite composite, but mercury intrusion porosimetry does not provide results for voids larger than 100 μm. Photograph of the specimen with andalusite aggregate after exposure to 1200 °C shows large crack that do not appear in the porosimetric curve (Fig. 6). Such

considerable cracking of the specimens was observed for composites neither with chamotte nor with quartz sand. Therefore, total porosity of the latter two composites is formed mainly by pores of size between 1 and 100 μm.

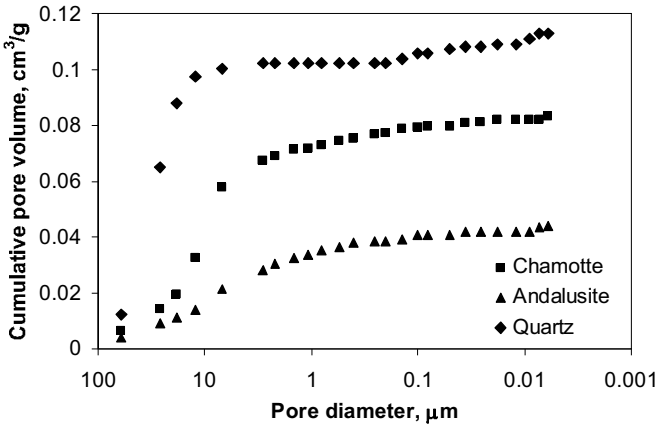

Fig. 5. Comparison of pore distribution of AAS composites after exposure to 1200 °C

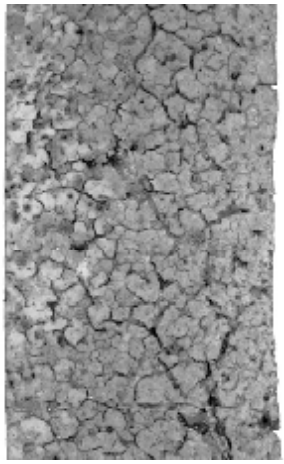

Fig. 6. Surface of andalusite composite specimen after exposure to 1200 °C

Alkali activated slag material exhibits amorphous gel structure at 20 °C. The contact zone between AAS paste and aggregate grains were studied by means of scanning electron microscopy. Presented micrographs show the contact zone of binder and aggregate grains of andalusite (Fig. 7) and chamotte, respectively (Fig. 8). Since surface of andalusite is quite flat, it is only sparsely connected to the binder and so it does not prevent the AAS matrix from significant drying shrinkage. This effect is predominantly responsible for crack formation and finally also for noticeable strengths' deterioration when compared to other composites. On the contrary, the surface of chamotte aggregate is so rugged that bonds with matrix are stronger and the composite is more compact.

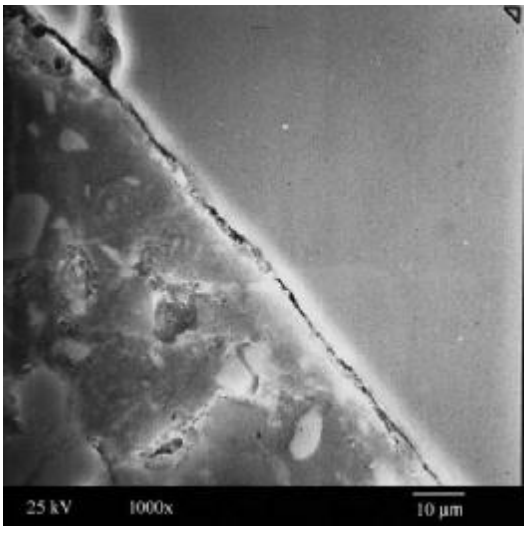

Fig. 7. SEM micrograph of AAS composite with andalusite

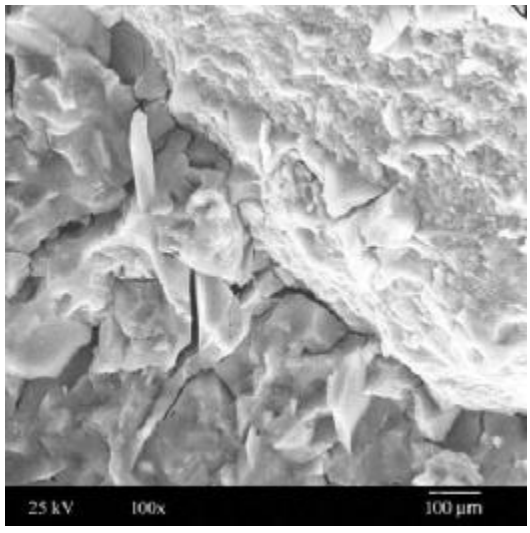

Fig. 8. SEM micrograph of AAS composite with chamotte

As the temperature increases, decomposition and further shrinkage of the AAS matrix can be observed, which implies enlargement of pores evoking spongy structure of the AAS paste. This weakening of AAS structure is the main reason for strengths' deterioration that has been discussed above. At temperature that reaches 1200 °C the formation of very strong connection between alkali activated slag and the surface layer of chamotte aggregate can be observed (Fig. 10). This ceramic bond is so strong that fracture of aggregate grains occurs during mechanical testing. Such sintering of aggregate with a binder in the contact zone does not occur either for quartz or andalusite type of aggregate (Fig. 9). This effect is also the main reason for enormous increase in especially flexural strength and better performance of composite material with chamotte aggregate after exposure to extremely high temperatures

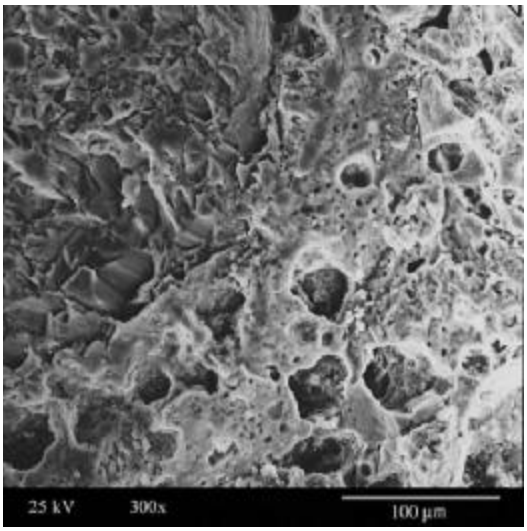

Fig. 9. SEM micrograph of AAS composite with andalusite after exposure to 1200 °C

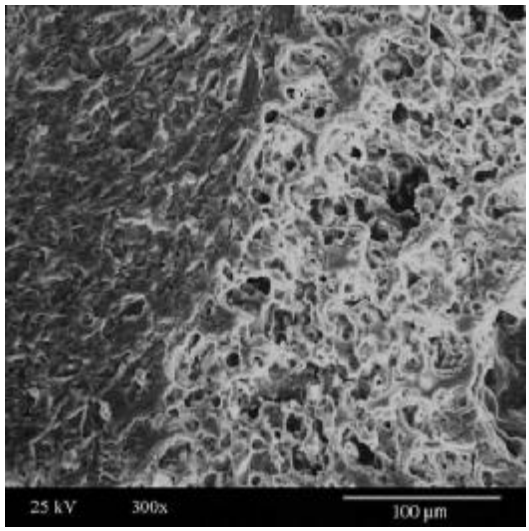

Fig. 10. SEM micrograph of AAS composite with chamotte after exposure to 1200 °C

3 SUMMARY AND ACKNOWLEDGMENT

The properties of alkali activated slag material and its behavior upon heating up to 1200 °C considerably depend on the type of aggregate that is used as filler. Alkali activated slag paste itself performs much better compared to concrete made of ordinary Portland cement when subjected to very high temperatures or fire but mechanical properties of this material are strongly affected by aggregates. It turned out that the main factor for good mechanical performance of AAS composites is the quality of interface between aggregate grains and binder. Stronger connection with aggregate mitigates the action of mechanical stress on binder that is caused by its shrinkage and it impedes the formation of larger cracks that contribute to strength's deterioration.

Utilization of chamotte as an aggregate in alkali activated slag composites seems to be the most effective among other studied aggregates. Chamotte is a material that is produced from natural clay in rotary kiln at 1350 °C, and therefore it is more thermally stable than quartz or andalusite. Quartz exhibits phase modification at 573 °C and andalusite forms very weak connection with AAS binder which results in the formation of large cracks. From the viewpoint of mechanical properties, chamotte aggregate does not limit mechanical strengths of AAS paste at temperatures up to 1000 °C and it even considerably improves the flexural strength of the composite at 1200 °C. Although some deterioration occurs upon heating, the compressive strength decreases to the limit of 29 MPa at 1000 °C. However, it is still 31% of the original strengths. The flexural strength falls to limit of 4.2

MPa at 800 °C, which is 40% of the original strength. All these very good properties predetermine chamotte aggregate especially in alkali activated slag composites for application in structures that might be exposed to elevated temperatures.

This paper was elaborated with the financial support of the project granted by Ministry of Education, Youth and Sport (MSM 0021630511).

REFERENCES

[1] Husem, M. The effects of high temperature on compressive and flexural strengths of ordinary and high-performance concrete, *Fire Safety Journal* 2006, vol. 41, 155-163.

[2] Li, M., Qian, C., Sun W. Mechanical properties of high-strength concrete after fire, *Cement and Concrete Research* 2004, vol. 34, 1001-1005.

[3] Kalifa, P., Menneteau, F.-D., Quenard D. Spalling and pore pressure in HPC at high temperatures, *Cement and Concrete Research* 2000, vol. 30, 1915-1927.

[4] Zuda, L., Rovnaník, P., Bayer, P., Černý, R. Effect of High Temperatures on the Properties of Alkali Activated Aluminosilicate with Electrical Porcelain Filler. *International Journal of Thermophysics* 2008, vol. 29, 693-705.

[5] Rovnaníková, P., Bayer, P., Rovnaník, P., Novák, J. Properties of Alkali-Activated Aluminosilicate Materials with Fire-Resistant Aggregate after High Temperature Loading. *Cement Combinations for Durable Concrete, Proceedings of the International Conference*. Dundee, UK: Dhir, R.K., Chana, P., Caliskan, S., Lavingia, R. (Eds.), Thomas Telford Ltd., London, UK, 2005, pp. 277–286.

[6] Rovnaník, P., Bayer, P., Rovnaníková, P. Utilisation of alkali activated aluminosilicates as fire protecting materials. In *Concrete for Fire Engineering, Proc. 7th Int. Congress – Concrete: Construction's Sustainable Option*. Dundee, UK: Dhir, R.K., Harrison, T.A., Newlands, M.D. (Eds.), IHS BRE Press, Brecknell, UK, 2008, pp. 273-282.

[7] Bayer, P. PhD thesis, Brno University of Technology, Brno 2005 (in Czech)

Application of Structural Fire Engineering, 19-20 February 2009, Prague, Czech Republic

THERMAL CONDUCTIVITY OF GYPSUM AT HIGH TEMPERATURES

A Combined Experimental and Numerical Approach

Ima Rahmanian [a], Yong Wang [a]

[a] University of Manchester, School of Mechanical, Aerospace and Civil Engineering, Manchester, UK

INTRODUCTION

Gypsum board based systems are now widely used in buildings, as walls or ceilings, to provide passive fire protection. The basis of the fire resistance of such systems lies in low thermal conductivity and the evaporation of the water content of the gypsum board, which absorbs a considerable amount of heat, thereby delaying temperature rise through the system. To accurately model the performance of such systems in fire condition, their thermal properties should be known. Thermal properties of gypsum are temperature-dependent and among them, thermal conductivity has a critical influence, but there is a wide difference in reported values in literature. Given the effects of porosity, non-homogeneity and moisture in gypsum, direct experimental measurement of thermal conductivity of gypsum at high temperatures is not an easy task. As an alternative, this paper proposes a hybrid numerical and experimental method to extract thermal conductivity of gypsum. A one-dimensional finite difference heat conduction programme has been developed to predict the temperature development through the thickness of the gypsum board, based on an initial estimate of the thermal conductivity-temperature relationship as a function of porosity and radiation within the voids. This relationship is then calibrated by comparing numerical results with the experimental ones from small-scale fire tests, so that the temperature history of the specimen calculated by the programme closely matches those recorded during the test. This method has been found to yield more consistent results than those reported in literature.

1 OUTLINE OF THE NUMERICAL ANALYSIS METHOD

The transient heat transfer through a gypsum board is modelled using one-dimensional Finite Difference formulation. A computer program has been developed and implemented in the familiar environment of Microsoft Excel using VBA. The modelling procedure has been thoroughly validated [1] by comparisons with a number of analytical solutions and simulation results using ABAQUS/Standard. The following describes the basis of the modelling method.

1.1 One-Dimensional Finite Difference Formulation

The Fourier's law of conduction in one dimension with no heat generation is expressed as:

$$\frac{\partial}{\partial x}\left(k(T)\frac{\partial T(x,t)}{\partial x}\right)=\rho c\frac{\partial T(x,t)}{\partial t} \tag{1}$$

where $T(x,t)$ is temperature (°C);
$k(T)$ is thermal conductivity (W/m.°C);
ρ is material density (kg/m^3);
c is specific heat of material (J/kg.°C);
t is time (sec);
x is the coordinate ($0 \le x \le L$, L being the thickness of the panel).

Choosing the explicit technique, the temperature of a volume cell (refer to *Figs 1* and *2*) at a time step is computed directly based on the temperatures of the adjacent cells in the last time step which leads to a very simple scheme of computation [2]:

(i) For a typical node m within the material (*Fig. 1*):

$$T'_m = F_0[\frac{2(k_{m-1,m}T_{m-1} + k_{m+1,m}T_{m+1})}{k_{m-1,m} + k_{m+1,m}} + T_m(\frac{1}{F_0} - 2)] \quad (2)$$

where F_0 is defined as: $$F_0 = \frac{(k_{m-1,m} + k_{m+1,m})\Delta t}{2\rho c(\Delta x)^2} \quad (3)$$

T'_m is the temperature of m in the subsequent time step and $k_{i,j}$ is the thermal conductivity at the average temperature of cells i and j: $$k_{i,j} = k(\frac{T_i + T_j}{2}) \quad (4)$$

Numerical stability under the explicit scheme requires: $$\Delta t \le \frac{\rho c(\Delta x)^2}{(k_{m-1,m} + k_{m+1,m})} \quad (5)$$

(ii) For a boundary node, when subjected to convective and radiative boundary conditions (*Fig. 2*):

$$T_1' = 2F_0[T_2 + \frac{h\Delta x}{k_1}T_\infty + (\frac{1}{2F_0} - 1 - \frac{h\Delta x}{k_1})T_1] + \phi E\sigma[(T_\infty + 273)^4 - (T_1 + 273)^4]\frac{2\Delta t}{\rho c\Delta x} \quad (6)$$

where F_0 is $F_0 = \frac{k_1\Delta t}{\rho c(\Delta x)^2}$

$h(T)$ is convection heat transfer coefficient (W/m^2.°C);
T_∞ is the ambient temperature (°C);
ϕ is a geometric "view factor"
E is the effective emissivity
σ is Stefan-Boltzmann constant (5.67x10^{-8} W/m^2.K^4).

Numerical stability limits the time step to:

$$\Delta t \le \frac{0.5\rho c(\Delta x)^2}{k_1}[1 + \frac{h\Delta x}{k_1} + \frac{\phi E\sigma\Delta x}{k_1}\cdot\frac{(T_1 + 273)^4}{T_1}]^{-1} \quad (7)$$

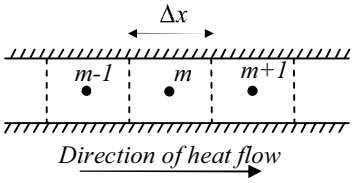

Fig. 1. Finite Difference discretization for node m within the material

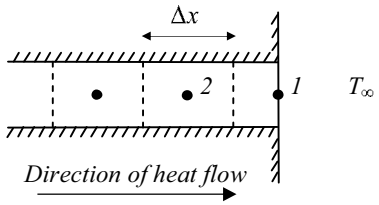

Fig. 2. Finite Difference discretization for a boundary node

1.2 Initial and Boundary Conditions

Gypsum board is assumed to have a uniform initial temperature equal to the ambient temperature. On the unexposed boundary, the convective heat transfer coefficient (h) is assumed to be constant and the value is taken as 10 W/m^2.°C. The surface of gypsum plasterboards is laminated by paper with emissivity of 0.8-0.9 as reported in reference [3]. Thus, the surface emissivity of the board is taken as 0.8 and the view factor equals unity. For extraction of thermal conductivity based on fire test results, the recorded temperatures on the exposed surface are used as input data.

1.3 Specific Heat and Density

The temperature-dependent specific heat of gypsum experiences two peaks corresponding to the two dehydration reactions of gypsum as shown in *Fig. 3*. These peaks represent the energy consumed to dissociate and evaporate water and include the effect of water movement and

recondensation of water in cooler regions of gypsum [4]. The base value of the specific heat is 950 J/kg.°C as reported by Mehaffey *et al* [5] and the additional specific heat at each dehydration reaction can be expressed by [4]:

$$\Delta c = \frac{2.26\times10^6}{\Delta T}(e_d f_1 + e_{free}) f_2 \quad \text{(J/kg.°C)} \tag{8}$$

where Δc is the average additional specific heat
e_d is the dehydration water content (percentage by total weight)
e_{free} is the free water content (percentage by total weight)
ΔT is the temperature interval
f_1, f_2 are correction factors to account for heat of reactions and effects of water movement

According to Ang and Wang [4], f_2=1.28 and 1.42 for the first and second dehydration reactions, respectively. For standard fire conditions f_2=1.4.

Due to evaporation of water, the density of gypsum reduces with temperature increase. *Fig. 4* shows the density used in the modelling as a percentage of the original density of gypsum at ambient temperature.

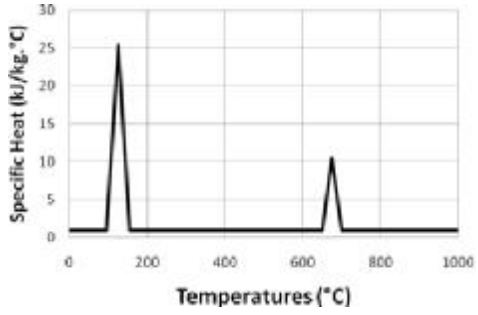

Fig. 3. Specific heat of gypsum as used in the analysis

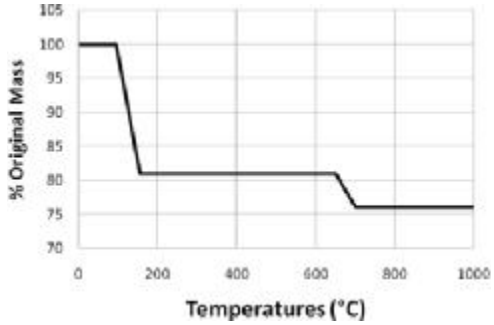

Fig. 4. Density of gypsum as used in the analysis (% of the original density)

1.4 Thermal Conductivity

Since gypsum is a porous material, heat transfer through gypsum is a combination of all three modes: conduction through the solid and convection and radiation through the pores. Therefore the effective thermal conductivity of gypsum should include these effects. This effective thermal conductivity can be affected by many factors such as temperature, density, moisture content and porosity of the material. Such sensitivity contributes to the diverse data reported in literature as demonstrated in *Fig.5*. Assuming gypsum is made of solid substrate and uniformly distributed spherical pores, the effective thermal conductivity of gypsum may be calculated using the following equation [6]:

$$k^* = k_s \frac{k_g \varepsilon^{\frac{2}{3}} + (1-\varepsilon^{\frac{2}{3}})k_s}{k_g(\varepsilon^{\frac{2}{3}} - \varepsilon) + (1-\varepsilon^{\frac{2}{3}} + \varepsilon)k_s} \tag{9}$$

where k^* is the effective thermal conductivity of gypsum
k_g is effective thermal conductivity of gas to account for heat transfer in the pores
k_s is the thermal conductivity of the solid
ε is the porosity of the material (the ratio of the volume of void to the overall volume)

In this study, the thermal conductivity of solid gypsum (k_s) is 0.12 W/m.°C. The porosity of gypsum is 0.25. Since the size of the pores is very small (never larger than 5mm), natural convection in the pores can be neglected. Therefore the effective thermal conductivity of the gas is [6]:

$$k_g = 4.815\times10^{-4}T^{0.717} + \frac{2}{3}\times 4 d_e \sigma T^3 \qquad (10)$$

where T is absolute temperature and d_e is the effective diameter of the pores. In this study d_e =1mm. Hence, the effective thermal conductivity-temperature relationship consists of three parts as demonstrated in *Fig. 6*: 1) Constant thermal conductivity up to 95°C before water evaporation, equal to that at ambient temperature reported by the manufacturer; 2) Linear reduction of conductivity to 0.1 W/m.°C at 155°C; 3) Non-linear increase in thermal conductivity based on equations 9 and 10.

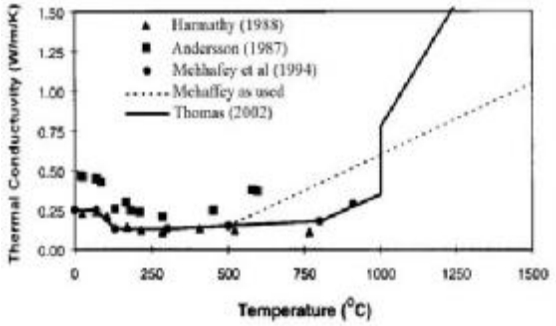

Fig. 5. Thermal conductivity of gypsum as reported by various researchers [7]

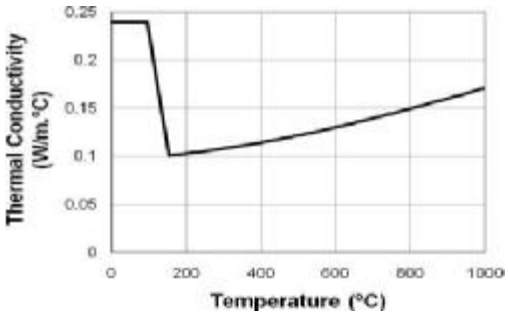

Fig. 6. Effective thermal conductivity of gypsum as used in this study

2 SMALL-SCALE HIGH TEMPERATURE TESTS

A limited number of small-scale experiments have been performed. The specimens tested were gypsum board panels of two different types; 12.5mm *Gyproc Fireline* plasterboard and 9.5mm *Gyproc Wallboard* plasterboard, both *British Gypsum* products. A total number of 8 specimens were tested as specified in *Table 1*. All specimens were with approximate dimensions of 400×400 mm. Each specimen was placed horizontally on top of an electric kiln, as the source of heat, so that one side of the panel was subjected to kiln temperature and the other side faced up to the room temperature (19-25°C). An opening of 280×265 mm on the top lid of the kiln allowed the lower side of the panel to be exposed to the elevated kiln temperatures. A 30mm layer of glass wool (with an opening of the same size as that in the kiln lid) was laid underneath the specimen to insulate the contact surface between the top lid and the plasterboard. *Fig. 7* shows typical set-up of the experiments. *Fig. 8* shows the heating curve achieved in the kiln which is compared to a standard cellulosic fire (BS476) [8]. Temperatures were measured on the unexposed side, the midpoint (for double layered panels) and the exposed side of the gypsum panel using Type K thermocouples.

Table 1. Specifications of gypsum board specimens

Test No	Plaster board Type	Layers	Total Thickness (mm)	Density (kg/m3)	Free Water (% by weight)	Initial Thermal Conductivity (W/m.°C)
1	Gyproc Fireline	Single	12.5	784	3.5	0.24
2	Gyproc Fireline	Single	12.5	784	3.5	0.24
3	Gyproc Fireline	Double	25	784	3.5	0.24
4	Gyproc Fireline	Double	25	784	3.5	0.24
5	Gyproc Wallboard	Single	9.5	663	3.5	0.19
6	Gyproc Wallboard	Single	9.5	663	3.5	0.19
7	Gyproc Wallboard	Double	19	663	3.5	0.19
8	Gyproc Wallboard	Double	19	663	3.5	0.19

Fig. 7. Typical set-up for the small-scale fire tests

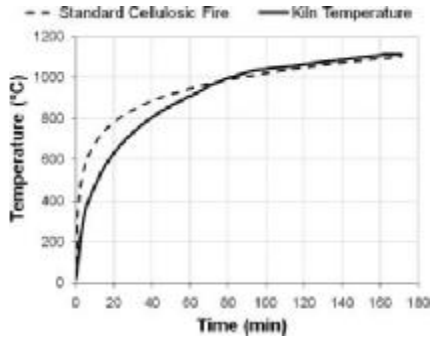

Fig. 8. Time-temperature curve for the kiln against standard cellulosic fire curve

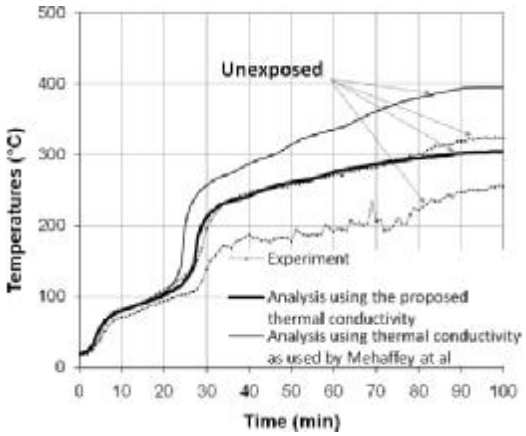

Fig. 9. Temperature history for 12.5mm Fireline gypsum panel

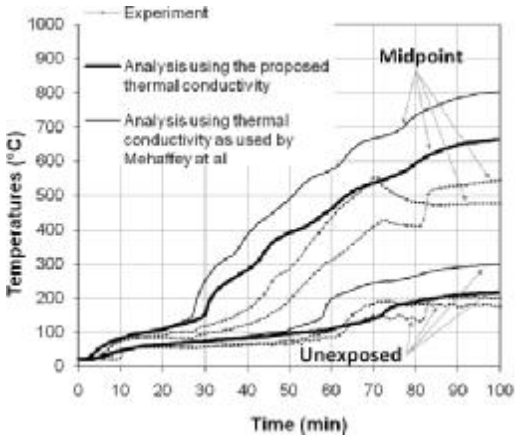

Fig. 10. Temperature history for 25mm Fireline gypsum panel

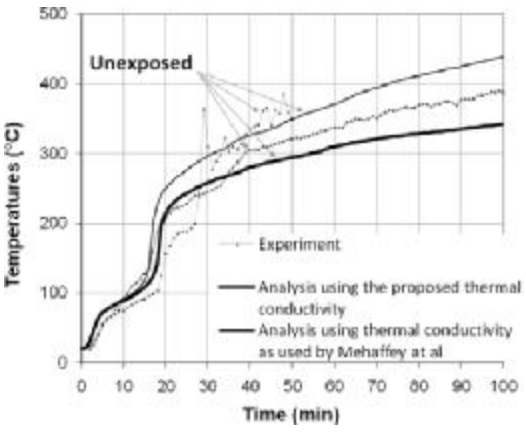

Fig. 11. Temperature history for 9.5mm Wallboard gypsum panel

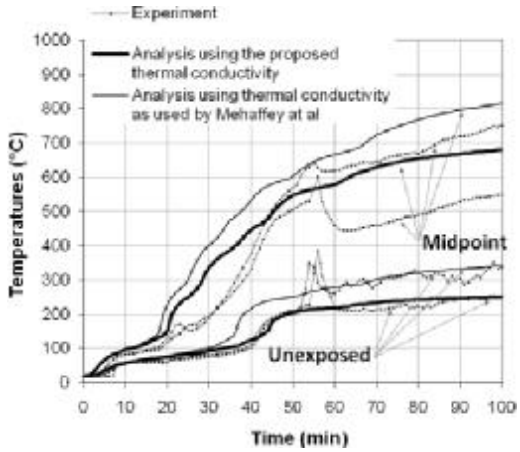

Fig. 12. Temperature history for 19mm Wallboard gypsum panel

3 RESULTS

In *Figs. 9* to *12*, the temperature histories measured from the tests (data points) and calculated by the program using pore size of 1mm (solid thick line) are compared. Also plotted in these figures are the numerical results utilizing thermal conductivity of gypsum as used by Mehaffey *et al* [5] (thin solid line). The results demonstrate a considerable improvement in prediction of temperature development through gypsum when using the new thermal conductivity model described in this paper.

4 CONCLUSIONS

This paper has presented a hybrid method to determine the effective thermal conductivity of gypsum at high temperatures, based on using small-scale experimental results and a thermal conductivity model which includes the effects of radiation in voids. Despite the simplicity of the method, the results are in good agreement with test measurements and show great improvement when compared to those produced using thermal conductivity values reported in literature. This method will aid manufacturers to develop their products without having to conduct numerous large-scale fire tests. Further planned research includes investigating the effects of discrete large cracks in gypsum on heat transfer in gypsum board systems and gypsum falling-off at high temperatures.

5 ACKNOWLEDGMENT

The authors would like to thank British Gypsum for their financial support and Drs. Kane Ironside and Jan Rideout for their interest and technical support. The technical assistance by the laboratory staff at the University of Manchester is greatly appreciated.

REFERENCES

[1] Rahmanian I., Fire Resistance of Gypsum Board Based Systems, First year PhD progression report, *School of Mechanical, Aerospace and Civil Engineering*, University of Manchester, UK, 2008

[2] Wang, H.B., Heat Transfer Analysis of Components of Construction Exposed to Fire, *Department of civil Engineering and Construction*, University of Salford, U.K., 1995

[3] Ozisik, M.N., Heat Transfer: A Basic Approach, New York; London: *McGraw-Hill*, 1985

[4] Ang, C.N. and Wang, Y.C., The Effect of Water Movement on Specific Heat of Gypsum Plasterboard in Heat Transfer Analysis Under Natural Fire Exposure, *Construction and Building Materials*, **18**: p. 505-515, 2004

[5] Mehaffey, J.R., Cuerrier, p., and Carisse, G.A., A Model for Predicting Heat Transfer Through Gypsum-Board/Wood-Stud Walls Exposed to Fire, *Fire and Materials*, **18**: p. 297-305, 1994

[6] Yuan J., Fire Protection Performance of Intumescent Coating under Realistic Fire Conditions, PhD Thesis, *School of Mechanical, Aerospace and Civil Engineering*, University of Manchester, UK, 2009

[7] Thomas, G., Thermal Properties of Gypsum Plasterboard at High Temperatures, *Fire and Materials*, **26**: p. 37-45, 2002

[8] BS476, Fire tests on building materials and structures, Part 20: Method for determination of the fire resistance of elements of construction (general principles), *British Standards Institution*, 1987

THERMAL CONDUCTIVITY OF GYPSUM PLASTERBOARDS

At ambient temperature and exposed to fire

A.C.J. de Korte, H.J.H Brouwers

University of Twente, Faculty of Engineering Technology, Department of Construction Management and Engineering, Enschede, The Netherlands

INTRODUCTION

One of the more complicated thermal properties to calculate for gypsum plasterboard is the thermal conductivity. The thermal conductivity is important because it plays an important role in the fire behaviour of gypsum plasterboards. Plasterboard often protects steel structures of buildings, because it conducts heat slowly and absorbs the heat of the fire by its volumetric enthalpy. This paper will focus on the first role.

The thermal conductivity becomes more complicated for porous media, which consist of different phases. Kaviany (1995) points out that the heat conduction through fully saturated matrix depends on the structure of the matrix and the thermal conductivity of each phase. The same principle applies for any heterogeneous material. One of the most difficult aspects of the analysis of heat conduction through a porous medium is the structural modelling. The thermal conductivity of the solid phase is generally larger then that of the fluid, the manner in which the solid is interconnected influences the conduction. Plasterboard consists of a solid phase and water/air mix in the voids. The thermal conductivity of the voids depends strongly on the amount of moisture (absorbed water) in the voids, since the thermal conductivity of water is 23 times the thermal conductivity of air.

This article will try to solve this problem partly by assuming that gypsum plasterboards can be assumed to be a three-phase system consisting of two different two-phase systems. This concept is applied to various types of gypsum/limestone plasterboards. The models are validated by comparing the results of the models with experiments. Based on these results and models conclusions are drawn in regard to the amount of absorbed water.

Finally the concept of thermal conductivity is applied on gypsum plasterboards under fire.

1 TWO-PHASE SYSTEMS

This section will focus on the description of thermal conductivity for two phase systems (fluid-solid). For these systems, several equations have been suggested during the last two centuries. Côte and Konrad (2008) point out that heat conduction through a two-phase porous media depends on the thermal conductivity as well as the structure of the solid matrix. In terms of thermal behaviour, the structure of the solid matrix determines the contact resistance and the continuity of the solid phase (Kaviany, 1995). Hamilton and Crosser (1962) showed theoretically that the thermal conductivity of particle packings decrease with increasing sphericity of particles. This effect was also noticed by Johansen (1975) and Côté and Konrad (2005) in air-saturated geomaterials where the thermal conductivity of natural particle packing (rounded/sub-rounded particles) were systematically lower than those of crushed particle packings (angular/sub-angular particles). A possible reason for this effect could be found in the smaller contact areas among the spherical particles compared to the more angular particles. Since the amount of contact area is related to the possible amount of solid-solid conductivity, which is always more than solid-fluid conductivity.

Within this article two equations are used, which take into account the structure of the solid. The first equation was introduced by Hadley (1986). This equation uses a so called mixture factor, which depends on the sphericity of the particles and the ratio of the thermal conductivity of the different phases. Another possibility is to describe the thermal conductivity with method of Zehner and Schlünder (1972). Zehner and Schlünder take into account the shape of the particles and therefore their surface connectivity. For the description of the form of the particle the factor C is used. These values are for particles which can be freely move in/through the matrix. In the case of a gypsum core there are a high number of so-called solid-phase bridges. This higher connectivity leads to a higher conductivity compared to a system with the same void fraction but with lower connectivity. For such systems with high number of solid-phase bridges, a C-value of 5 is proposed (Zehner and Schlünder, 1970).

2 THEORY VERSUS EXPERIMENTAL DATA

This section describes the experimental data on thermal conductivity of gypsum plasterboards found in literature, which are used to compare with the results of the theoretical equations. This experimental data is often found together with a description of the apparent density and chemical composition. Both these parameters are important in order to predict the thermal conductivity of plasterboards. The density is important because it is closely related to the void fraction of plasterboards. As can be seen in the previous section, the void fraction is one of the main parameters for the calculation of the thermal conductivity. The chemical composition of gypsum plasterboards influences the thermal conductivity of the solid phase within the board.
Table 1 shows values which are presented in literature. The experimental data is compared with the equations of the previous section. For this comparison the thermal conductivity of the solid needs to be known. Since the solid phase of gypsum plasterboards consist of several phases, the thermal conductivity of the solid phases has to be calculated. There are different calculation methods available for thermal conductivity of the composite solid.

Table 1. Experimental values of gypsum plasterboards as describes in literature

Source	**Apparent density**	**Composition**			k_{meas}
	ρ_e	$\%m_{C\bar{S}H_2}$	$\%m_{C\bar{C}}$	$\%m_{M\bar{C}}$	
	[kg/m^3]	[kg/kg]	[kg/kg]	[kg/kg]	[W/(m K)]
Wullschlager (2008)	810	81	9.5		0.28
Ang and Wang (2004)	836.4				
Grazi Wakali (2007)	810	81	9.5		0.28
Mehaffey (1994) 1	732				0.25
Mehaffey (1994) 2	648				0.24
Clancy (2001)					0.18
Sultan (1996)	698				0.25
Thomas (2002)					0.25
Ghazi Wakali (2008) 1	735	80.9	12.3		0.28
Ghazi Wakali (2008) 2	840	62.2	32.3		0.30
Ghazi Wakali (2008) 3	740	76.5	4.2	4.7	0.23
Ghazi Wakali (2008) 4	870	98			0.32

The geometric mean (eq. (1)) is a type of average, which indicates the central tendency or typical value of a set of numbers, and is often used for exponential data. As it is the most realistic model, it is used for the calculation of the solid thermal conductivity. Côté and

Konrad (2005) recommend this geometric method for the calculation of the thermal conductivity of dry soil. The method uses the volume-based composition. This equation reads;

$$k_s = \prod k_i^{\delta_i}, \qquad (1)$$

with k_i is the thermal conductivity of i^{th} phase and δ_i the volume fraction of i^{th} solid phase. Table 4 shows the results of the thermal conductivity of the solid phase based on eq. (1), the chemical composition from Table 1 and properties from Table 2.

Table 2. Thermal conductivities and specific density

Substance	**Thermal conductivity** [W/(m K)]	**Specific density** [kg/m^3]
$CaSO_4 \cdot 2H_2O$	1.255	2310
$CaCO_3$	3.58	2720
$MgCO_3$	5.83	2990
H_2O	0.60	1000
Air (dry)	0.026	1.3

Table 3. The solid thermal conductivity for the solid phase only based on the geometric method and the solid composition

	Solid thermal conductivity [W/(m K)]
Wullschlager (2008)	1.38
Mehaffey (1994) 1	1.26
Mehaffey (1994) 2	1.26
Sultan (1996)	1.26
Grazi Wakali (2008) 1	1.42
Grazi Wakali (2008) 2	1.72
Grazi Wakali (2008) 3	1.40
Grazi Wakali (2008) 4	1.26

Next, the two-phase conductivities are computed based on the expressions from Section 1 and the calculated solid thermal conductivities from Table 3. The results of these computations are presented in Table 4.

Table 4. Results of different theoretical equations for the dry thermal conductivity

	k_{meas}	**Zehner and Schlünder (1972)**
Wullschlager (2008)	0.28	0.171
Wullschlager (2008)	0.28	0.165
Wullschlager (2008)	0.28	0.167
Mehaffey (1994) 1	0.25	0.145
Mehaffey (1994) 2	0.24	0.126
Sultan (1996)	0.25	0.137
Grazi Wakali et al (2008) 1	0.28	0.152
Grazi Wakali et al (2008) 1	0.28	0.146
Grazi Wakali et al (2008) 1	0.28	0.149
Grazi Wakali et al (2008) 2	0.30	0.189
Grazi Wakali et al (2008) 2	0.30	0.175
Grazi Wakali et al (2008) 2	0.30	0.181
Grazi Wakali et al (2008) 3	0.23	0.154
Grazi Wakali et al (2008) 3	0.23	0.147
Grazi Wakali et al (2008) 3	0.23	0.149
Grazi Wakali et al (2008) 4	0.32	0.181

The best results were obtained with Zehner and Schlünder with C = 5 [1]. The obtained value from the equation of Zehner and Schlünder (1972) are too low compared to the results obtained from experiments. This could be the result of the current assumption that the voids

[1] A comparison of more equations and the experimental data can be found in De Korte and Brouwers (2009).

are filled with dry air, while in reality the fluid in the voids is usually moistured. Building materials, like gypsum plasterboards, are porous media in which moisture transfer occurs in both the vapor/gas and liquid phase. Bouguerra (1999) points out that the thermal conductivity is strongly influenced by the moisture content migrating through porous material. Since the thermal conductivity of water vapour is similar to the thermal conductivity of air there will no clear difference. But the thermal conductivity of liquid water is 23 times the thermal conductivity which will lead to clear difference. The next section will focus on the effect of moisture on the thermal conductivity of the gypsum plasterboards.

3 THREE-PHASE SYSTEM

This section will focus on the calculation of the thermal conductivity of a solid porous medium with a mixture of a liquid (water) and a gas (dry air) in the voids. Somerton et al. (1973) have derived the following equation for porous medium filled by a mixture of two fluids

$$k_e = k_g + \sqrt{s_l}(k_l - k_g) \quad . \tag{2}$$

Here k_g is the effective thermal conductivity of the porous medium filled with dry air, k_l is the effective thermal conductivity of the porous medium filled with water and s_l is the water saturation in the voids. Both k_g and k_l can be calculated with the equations for two-phase effective conductivity given in Section 2, with k_{air} and k_{water} as the k_f respectively.
Here, this method proposed by Somerton et al. (1973) is used to derive the amount of water needed to comply with the thermal conductivity as measured in the literature. During this derivation the effect of the moisture on density needs to be taken into account. A higher moisture content means a lower dry mass, so lower dry density. The dry density, in turn, is related to the void fraction of the material. So the density, void fraction and moisture content are all interrelated.
Table 5 shows the results of both the Zehner & Schlünder equation The sorbed water values are all in line with values from literature. Ang and Wang (2004) also give a moisture content of 3% m/m. This value is furthermore mentioned by Thomas (2002), Belmiloudi and Le Meur (2005). Therefore one can conclude that all three equations are close to the values from literature.

Table 5. Water content derived to match the experimental value

	Zehner & Schlünder C=5
Wullschlager (2007)	2.08 %
Mehaffey (1994) 1	2.32 %
Mehaffey (1994) 2	3.42 %
Sultan (1996)	2.95 %
Ghazi Wakali (2008) 1	3.37 %
Ghazi Wakali (2008) 2	1.72 %
Ghazi Wakali (2008) 3	1.78 %
Ghazi Wakali (2008) 4	3.24 %

4 APPLICATION TO THERMAL CONDUCTIVITY DURING FIRE

In the previous sections the thermal conductivity at ambient temperatures were analysed. In this section, the developed method is used for the determination of the thermal conductivity during fire, i.e. for elevated temperatures.

The thermal conductivities can be computed as the composition of the system is known for all temperatures. The decomposition process is described in more detail in de Korte and Brouwers (2009). Figure 1 shows the comparison of the results of the three-phase system with the experimental results of Mehaffey (1994). The used gypsum plasterboard of Mehaffey (1994) has a density of 732 kg/m^3 and consists of 100% gypsum. The thermal conductivity is simulated with the Zehner and Schlünder equation with a shape-factor (C) of 5 and an initial moisture content of 2.8% on the gypsum mass is used. This is based on the result from Section 3. The equation of Zehner and Schlünder is used because it depends on a few parameters. Furthermore the thermal conductivities of the solid and fluid phases are assumed to be equal to the data in Table 2, so the thermal conductivities are assumed to be constant, i.e. not a function of temperature. Also the thermal expansion of the solids is ignored. Upon heating, the solids expand, which reduces the void fraction.

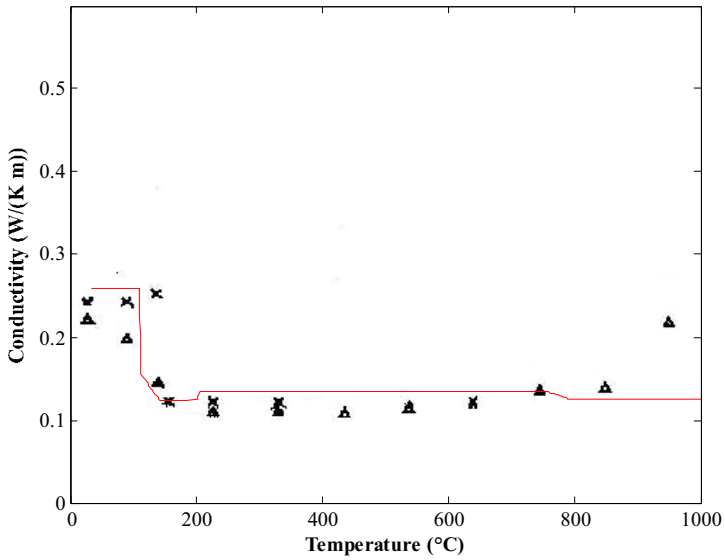

Fig. 1. Simulated thermal conductivity according to the proposed model (thin line) and experimental thermal conductivity (Mehaffey, 1994).

Notwithstanding these and other simplifications, it can be seen from Figure 1 that the simulated value have a good fit with the experimental value obtained from literature. The raise in thermal conductivity beyond 850°C in the experiments is probably caused by shrinkage cracks in the material. Due to cracks the air flows through the cracks more easy, increasing the apparent thermal conductivity. Obviously, this system change is not dealt with by the present model.

5 SUMMARY/CONCLUSION

The thermal conductivity of gypsum plasterboard up to a temperature of 105°C can be described best by a three-phase system as first introduced by Somerton et al (1973). This method requires information about the thermal conductivities which are provided by two-phase systems and the saturation of the voids. The two two-phase systems govern the cases with no saturation and full saturation of the voids.

For the two-phase system the Zehner and Schlünder equation met shape-factor of 5 yields good results. Furthermore, a moisture content of 2.8 % on plasterboard mass appears to be needed to explain the thermal conductivity of the board.
Using this moisture content of 2.8%, and the equations of Zehner and Schlünder with C=5 and Somerton, measured values for the thermal conductivity of several plasterboards from literature up to 105°C can be predicted excellently. This amount of moisture content is in line with the values reported in literature, and here it appears to depend only on the gypsum content of the solid phase. For more elevated temperatures, the two-phase equations (air/solid) also proves to be useful, when one takes account of the appropriate changes in the type of solid (dehydration, decarbonation) and volume (void fraction).

ACKNOWLEDGEMENTS

The author wishes to express their sincere thanks to the European Commission (I-SSB Project, Proposal No. 026661-2) and the following sponsors of the research group: Bouwdienst Rijkswaterstaat, Rokramix, Betoncentrale Twenthe, Betonmortelcentrale Flevoland, Graniet-Import Benelux, Kijlstra Beton, Struyk Verwo Groep, Hülskens, Insulinde, Dusseldorp Groep, Eerland Recycling, Enci, Provincie Overijssel, Rijkswaterstaat Directie Zeeland, A&G Maasvlakte, BTE, Alvon Bouwsystemen and V.d Bosch Beton (chronological order of joining).

REFERENCES

Ang, C. N., and Wang, Y. C. (2004). The effect of water movement on specific heat of gypsum plasterboard in heat transfer analysis under natural fire exposure. Construction and Building Materials, 18(7), 505-515.

Belmiloudi, A., and Le Meur, G. (2005). Mathematical and numerical analysis of dehydratation of gypsum plasterboards exposed to fire. Applied Mathematics and Computation, 163(3), 1023.

Bouguerra, A. (1999). Temperature and moisture dependence on the thermal conductivity of wood-cement-based composite: experimental and theoretical analysis. Journal of Physics D: Applied Physics, 32, 2797-2803.

Côté, J., and Konrad, J. M. (2008). Assessment of structure effects on the thermal conductivity of two-phase porous geomaterials. International Journal of Heat and Mass Transfer, Accepted.

de Korte, A.C.J. and Brouwers, H.J.H. (2009). Thermal conductivity of gypsum plasterboards. Submitted to Fire and Materials.

Grazi Wakali, K. and Hugi, E (2008) Four types of gypsum plaster boards and their thermo-physical properties under fire condition. Submitted to Journal of Fire Sciences.

Hadley, G. R. (1986). Thermal conductivity of packed metal powders. International Journal of Heat and Mass Transfer, 29(6), 909-920.

Hamilton, R. L., and Crosser, O. K. (1962). Thermal Conductivity of Heterogeneous Two-Component Systems. Industrial & Engineering Chemistry Fundamentals, 1(3), 187-191.

Johansen, O. (1975). Varmeledningsevne av jordarter, Ph.D. Thesis, Norge tekniske hogskole, Trondheim, Norway.

Kaviany, M. (1995). Principles of Heat Transfer in Porous Media (Second ed.). Springer, Berlin.

Mehaffey, J. R., Cuerrier, P., & Carisse, G. (1994). A model for predicting heat transfer through gypsum-board/wood-stud walls exposed to fire. Fire and Materials, 18(5), 297-305.

Somerton, W. H., Chu, S. L., & Keese, J. A. (1973). Thermal behavior of unconsolidated oil sands. Soc. Pet. Eng. AIME, Pap, 4506(48).

Sultan, M. A. (1996). A model for predicting heat transfer through noninsulated unloaded steel-stud gypsum board wall assemblies exposed to fire. Fire Technology, 32(3), 239-259.

Thomas, G. (2002). Thermal properties of gypsum plasterboard at high temperatures. Fire and Materials, 26(1), 37-45.

Wullschleger, L., and Wakili, K. G. (2008). Numerical parameter study of the thermal behaviour of a gypsum plaster board at fire temperatures. Fire and Materials, 32(2), 103-119.

Zehner, P. and Schlünder, E. U. (1970). Thermal conductivity of granular materials at moderate temperatures. Chemie Ingenieur Technik, 42(14), 933–941.

Zehner, P., & Schlünder, E. U. (1972). Einfluß der Wärmestrahlung und des Druckes auf den Wärmetransport in nicht durchströmten Schüttungen Chem. Ing.-Tech, 44(23), 1303-1308.

EFFECTIVE CHARACTERISTICS OF FIRE PROTECTION

Michal Strejček [a], Richard Cinař [a], Vilém Stanke [b], František Wald [a]

[a] Czech Technical University, Faculty of Civil Engineering, Prague, Czech Republic
[b] Promat a.s., Prague, Czech Republic

INTRODUCTION

Reliability of a steel structure exposed to fire conditions depends basically on the affect of mechanical and thermal actions. To predict the behaviour of the structure during the fire the gas temperature in the compartment, the temperature transfer into the structure element, the mechanical loading during the fire and the mechanical resistance of the structure is calculated. The collapse of the structural element occurs at the moment of reaching the critical temperature in the structure. High thermal conductivity of structural steel is the main disadvantage which causes the fast growth of the temperature in structural element. Application of the fire protection materials directly on the steel element can significantly affect the temperature growth. Thereby the structural collapse can be put behind.

Fig. 1 The fire test of Promapaint SC, see [7]

A number of fire protection materials are available to provide required fire resistance of the structure. Commonly used fire protection materials for structural steelwork include, except for traditional concrete protective layer, board type products, sprayed fire-resistive materials, thin-film intumescents materials and intumescent mat wrap materials, see [1]. All these materials are required to assure thermal insulation and carry its integrity at elevated temperatures during the fire. Selection of the specific type of fire protection material is managed by many factors, which classifies fire protection ability, durability, maintenance and aesthetic factor. Intumescent materials are ideal choice for uncovered members of steel structures. They are directly applied on the steel structure in thin layer from 450 to 2500 μm,

depending on required fire resistance of the structure. At elevated temperatures the thin layer goes through a chemical process, which causes the foaming. Initial layer is able to change its thickness more than 30 times during the heating. Foamed layer can provide the fire resistance commonly up to 2 hours. Board type products and sprayed fire-resistive materials are usually applied in cases of completely hidden structure. Board products, which are currently most used in commercial buildings, can provide the fire resistance up to 3 hours. Modern mixtures, improved by the reinforce fibres, ensure its integrity at high temperatures. Dry process during the construction and shape variability are their main advantages. Sprayed fire-resistive materials can be divided into two categories depending on the mixture which widely affect, except for the layer thickness, the fire resistance rating. Sprayed mineral fibre and sprayed cementitious mixtures can be recognized. Taking into account their mechanical and weather resistance are appropriate for offshore and industrial structures.

Temperature calculation of the structure during the fire can be described by a number of different ways. Prediction by the manufacturer´s table values, verified experimentally, is the most used method in established practice. Analytical design models, which provide more specific solution, are used in this article for temperature calculations of thermally protected steel elements. In spite of using the finite element approach is the most fitting method, remains this solution, due to its complicated calculation, in field of research.

1 ANALYTICAL MODEL

The temperature growth in the structural steel element can be delayed against the gas temperature in the fire compartment by using the fire protection material covering the structure. The temperature evaluation for a structural element protected by a thermal insulation layer includes considering the thermal equilibrium of heat emitted by hot gases, heat absorbed by the protection material and heat absorbed by the structural element. The heat is transferred through the insulation layer by conduction and the temperature increase $\Delta\theta_{a,t}$ during a time interval Δt can be obtained from Eq. (1) expecting uniform temperature distribution in cross-section [2].

$$\Delta\theta_{a,t} = \frac{\lambda_p A_p / V}{d_p c_a \rho_a} \frac{\theta_{g,t} - \theta_{a,t}}{1+\phi/3} \Delta t - \left(e^{\phi/10} - 1\right)\Delta\theta_{g,t}, \text{ but } \Delta\theta_{a,t} > 0 \qquad (1)$$

with:

$$\phi = \frac{c_p \rho_p}{c_a \rho_a} d_p \frac{A_p}{V}$$

where: λ_p is thermal conductivity of the fire protection material [J kg^{-1}K^{-1}]; A_p / V is the section factor of insulated steel member [m^{-1}]; $\theta_{g,t}$ is the ambient gas temperature at time t [°C]; $\theta_{a,t}$ is the steel temperature at time t [°C]; d_p is the thickness of the fire protection material [m]; c_p and c_a are specific heat of the fire protection material and of steel [J kg^{-1}K^{-1}]; ρ_p and ρ_a are unit mass of the fire protection material and of steel [kg/m^3]; $\Delta\theta_{g,t}$ is the gas temperature increase during the time interval Δt [K], where value of Δt should be considered less than 30 seconds. Recommended equation is useless for section factor A_p / V less than 10 m^{-1}. With A_p / V ratio higher than 350 m^{-1} it has not practical sense, because the element temperature equals to the gas temperature, $\theta_{a,t} \approx \theta_{g,t}$.

The temperature growth depends basically on thermal properties of the fire insulation layer, its thickness and on the A_p/V ratio, where A_p is inner surface of the insulation layer. The fire protection material is exposed to significant chemical process during the heating, which considerably changes its material characteristics. Conservative values of different materials at respective temperatures, determined from experimental results, are shown in Tab. 1, see [3].

For perfect prediction of the temperature growth in the steel member is necessary to take into account the material characteristics changes. The temperature inconsistency limits practical usage of analytical prediction model mentioned above. Values of material characteristics at respective temperatures can be replaced by an effective value.

2 EFECTIVE CHARACTERISTICS

Two fire tests in FIRES s.r.o. laboratory in Batizovce (Slovakia) were prepared to study the temperature increase in the steel element protected by boards PROMATEC ®-H and sprayed material TERFIX-P, see [4] and [5]. The temperature growth was observed during the heating in steel elements of different section factor and different thickness of thermal insulation. The gas temperature in the test furnace followed nominal standard fire curve.

Tab. 1 Properties of the enclosure surface materials at elevated temperatures

Material	Temperature θ °C	Unit mass ρ_p kg/m^3	Thermal conductivity λ_i W m^{-1} K^{-1}	Specific heat c J kg^{-1} K^{-1}	Coefficient $b=\sqrt{\rho c \lambda}$ J m^{-2} s$^{-1/2}$ K^{-1}
Normal concrete	20	2300	2,00	900	2030
	200	2300	1,63	1022	1960
	500	2300	1,21	1164	1800
	1000	2300	0,83	1289	1570
Steel	20	7800	54	425	13380
	200	7800	47	530	13940
	500	7800	37	667	13870
	1000	7800	27	650	11700
Gypsum insulating material	20	128	0,35	800	190
	200	128	0,06	900	80
	500	128	0,12	1050	130
	1000	128	0,27	1100	190
Sealing cement	20	200	0,0483	751	90
	250	200	0,0681	954	110
	450	200	0,1128	1052	150
	1050	200	0,2016	1059	210
CaSi board	20	450	0,0685	748	150
	250	450	0,0786	956	180
	500	450	0,0951	1060	210
	800	450	0,157	1440	320

Results of the test for boards PROMATEC®-H of minimal thickness 8 mm are compared to analytical prediction Tab. 2. Analytical prediction was realized based on effective material characteristics of the boards. The thermal conductivity development at elevated temperatures can be described by its effective value $\lambda_{p,eff}$. From experimental results were identified ideal values of the thermal conductivity at respective temperatures. Using the method of least squares the effective thermal conductivity formula for every board thickness can be derived, see *Fig 1*. For PROMATEC®-H boards with nominal thickness 7,6 mm the effective thermal conductivity is $\lambda = 3\times10^{-7}\,\theta_{a,t}^{\,2} - 0{,}0001\;\theta_{a,t} + 0{,}14$; where $\theta_{a,t}$ is the steel temperature.

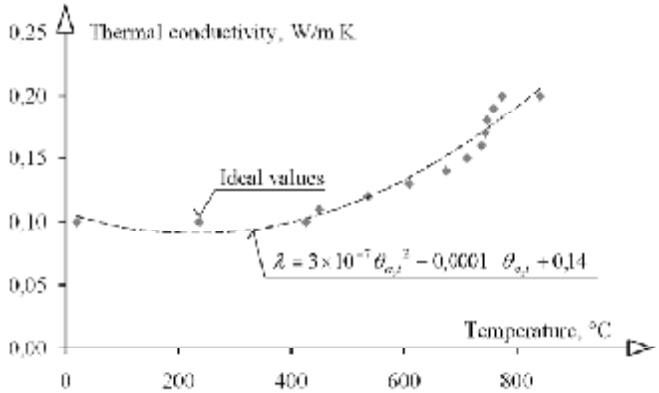

Fig. 2 Effective value of thermal conductivity $\lambda_{p,eff}$ for PROMATEC®-H, thickness 7,6 mm

Temperature prediction during the fire is slightly conservative, see Fig. 2. Black circular points represent manufacturer´s table values, see [6]. Conservative prediction in 30th min of the fire can be noticed.

Tab. 2 Test temperature compared to analytical prediction for PROMATEC®-H

		EXPERIMENT		ANALYTICAL MODEL			
Time [min]	ISO curve [°C]	Gas temperature [°C]	Element temperature [°C]	C_a [J/Kg°C]	C_p [J/Kg°C]	$\lambda_{p,eff}$ [W/mK]	Element temperature [°C]
0	20	35	23	440	800	0,000	20
5	576	357	72	450	838	0,137	39
10	678	679	122	482	875	0,133	97
15	739	729	189	516	913	0,132	172
20	781	779	257	541	950	0,133	239
25	815	809	322	563	988	0,137	302
30	842	838	385	586	1025	0,142	361
35	865	864	445	612	1063	0,150	417
40	885	889	498	642	1100	0,158	470
45	902	901	551	678	1138	0,168	519
50	918	913	600	718	1175	0,178	564
55	932	927	642	761	1213	0,188	606
60	945	942	680	799	1250	0,199	644
65	957	960	713	877	1288	0,210	680
70	968	978	738	1096	1325	0,220	711
75	979	978	762	2318	1363	732	732

An analytical prediction of temperature development in steel element protected by sprayed coating TERFIX-P was realized using the effective value of thermal conductivity which was derived from experimental results. Comparison of experimental measured temperature and predicted temperature is shown in *Fig. 4*. An inaccurate prediction can be noticed until 15th minute. Manufacturer´s table values are inaccurate in 30th min.

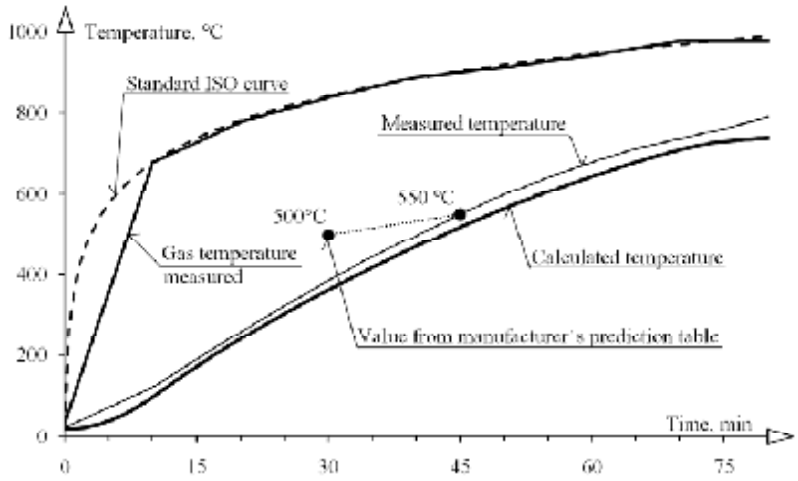

Fig. 3 Comparison of the measured temperature and calculated temperature for PROMATEC®-H boards of thickness d_p = 7,6 mm

Intumescent painting, except its density, thermal conductivity and specific heat, also changes its thickness. To determination of effective thickness was tested PROMAPAINT® -SC intumescent painting on opened and box cross-section columns in experimental furnace in laboratory Veselí nad Lužnicí, Czech Republic, see [7]. Three thicknesses were observed during the loading by a Standard fire curve: thin $d_{dry,thin}$ = 470 μm, medium $d_{dry,medium}$ = 1200 μm and thick $d_{dry,thick}$ = 2500 μm. Analytical prediction of temperature development in opened cross-section HEA 300 column covered with thin layer of intumescent painting is demonstrated in Fig. 5. For minimal initial thickness $d_{dry,min}$ = 470 μm was derived an effective thickness $d_{p.eff}$ = *8* mm. Other material characteristics were considered constant with values of density ρ_p = 350 kg/m^3, thermal conductivity γ_p = 0,20 W m^{-1}K^{-1} and specific heat c_p = 1100 J kg^{-1}K^{-1}. An inaccurate prediction until 15th minute of the fire is caused by time-delayed of the foaming. Effective thickness for medium and thick initial layer can be considered by 18 and 20 mm.

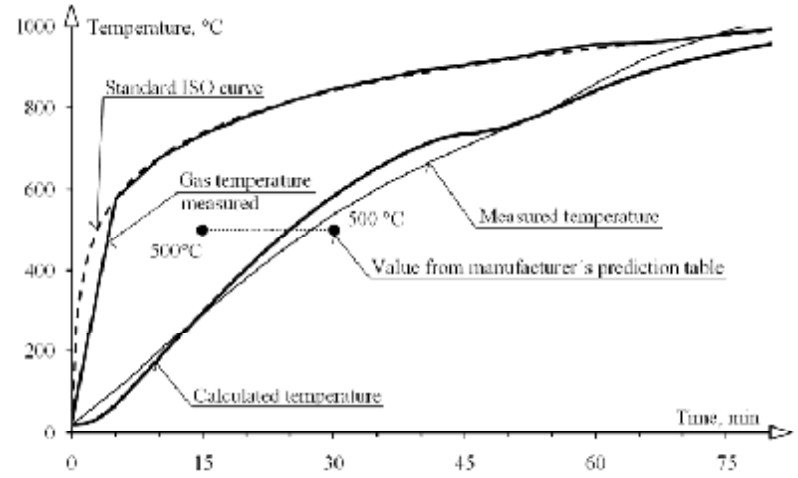

Fig. 4 Comparison of the measured temperature and calculated temperature for sprayed coating TERFIX-P of thickness d_p = 7 mm

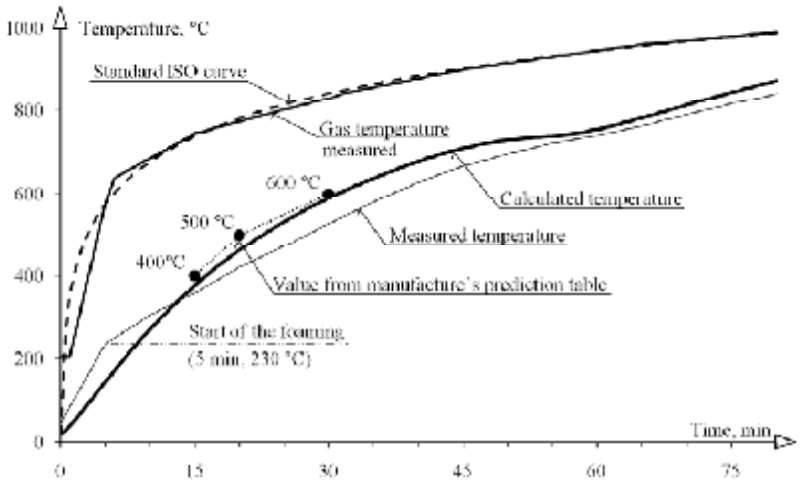

Fig. 5. Comparison of the measured temperature and calculated temperature for Promapaint SC intumescent painting using effective thickness $d_{p.eff}$ = 8 m

3 SUMMARY AND ACKNOWLEDGMENT

The calculations of the heat transfer to structures protected against fire are based on experimentally verified times of the completeness of fire protection elements. Thermal properties can be determined conservatively using nominal values shown in the respective tables or more accurately by evaluating the tests. The contribution documents a good accuracy of the analytical prediction for commonly used fire protection materials.

The authors would like to thank PROMAT a.s. and TORA s.r.o. for publishing of the experimental results.

REFERENCES

[1] Parker A.J., Beitel J.J., Iwankiw N.R., Fire Protection Materials for Architecturally Exposed Structural Steel (AESS), *STRUCTURE magazine, 2005.*

[2] EN 1993-1-2:2005, Design of steel structures – Part 1-2: General rules – Structural fire design, *European Committee for Standardization*, Brussels, 2005.

[3] Vassart, L.G., Cajot, L.G., Brasseur, M., Thermal & Mechanical Actions – Part 1, DIFISEK^{+}, www.difisek.eu, 2007.

[4] Gorlický M., Protocol of the test, in Slovak Protokol o zkoušce FIRES FR 018/04CP, obklad ocelových konstrukcí, Typ PROMATEC$^{®}$-H, No. 415 a 445, Batizovce, Slovakia, 2004.

[5] Gorlický M., Protocol of the test, in Slovak Protokol o zkoušce FIRES FR 057/04CP, nástřik ocelových konstrukcí, Typ TERFIX P, Batizovce, Slovakia, 2004.

[6] Design tables of products PROMAT s.r.o., Praha, 2005, www.promatpraha.cz

[7] Louma, M., Protocol of the fire test resistance, in Czech Protokol o zkoušce požární odolnosti, Pavus a.s., protocol č. Pr-06-2.019, Veselí nad Lužnicí, 2006.

[8] Wald, F., Strejček, M., The effective properties of the fire protection materials, in Czech Účinné vlastnosti požárně ochranných materiálů, *Konstrukce*, roč. 6, č. 5, pp. 29 - 31. ISSN 1213 8762, 2007.